UNIVERSITA' DEGLI STUDI DI MILANO
Facoltà di Medicina e Chirurgia
Dipartimento di Scienze Biomediche per la Salute
Scuola di Dottorato in Scienze Morfologiche e Fisiologiche
XXV ciclo

SGLT-1: A NEW THERAPEUTIC STRATEGY TO MAINTAINS INTESTINAL EPITHELIAL INTEGRITY AND BARRIER FUNCTION

Settore Disciplinare BIO16

Tutor: Prof. Cristiano Rumio
Coordinatore: Prof.ssa Laura Vizzotto

Tesi di Dottorato di Ricerca di
Diego Cardani
Matr. R08679

Anno Accademico 2012-2013

INDEX

1. INTRODUCTION

1.1 EPITHELIAL BARRIER: THE IMPORTANCE OF BEING INTACT

Epithelial barrier and its role in intestinal homeostasis maintenance

Pluricellular organisms interface with their external environments at multiple sites, including mucosae of the airway, oral cavity, digestive tract and genitourinary tract, and the skin. Although the skin is the most visible site of interface, the combined area of the mucosal surface is much greater than that of the skin. Epithelial cells that define the interface between the organism and external world forms barriers that are essential to life.

This is particularly true in the intestine, where the epithelial barrier supports nutrient and water transport while preventing microbial contamination of the interstitial tissue.

Gut epithelial surfaces are composed of cells lineages that arise from a pluripotent stem cell progenitor: absorptive enterocytes, globet cells, enteroendocrine cells and Paneth cells (1). All cellular types contribute in a unique way to mucosal defense and the maintenance of barrier integrity. Goblet cells, both the small and large intestines, secrete mucus, which is composed mainly of highly glycosylated proteins that form a protective layer on the epithelium surface. Mucus acts trapping the vast majority of antigens that, in the intestinal tract, are cleared by peristalsis. By keeping microbes moving, these physical factors limit the time available for adherence to the epithelia and thus restrict invasion. The importance of mucus gel hydration is shown by cystic fibrosis, in which the production of hyper-viscous mucus contributes to pulmonary, pancreatic and intestinal disease (2). Defective mucus production has also been reported in various immune-mediated diseases, and spontaneous colitis develops in mice that lack specific mucin genes (3).

In the small intestine, Paneth cells are the key effectors of antimicrobial defense. These specialized epithelial cells are situated at the base of small intestinal crypts and harbor secretory granules containing several microbicidal proteins including defensins, lysozyme, and phospholipase A2. Paneth cells sense bacterial proximity and react by discharging

their microbicidal granule contents into the gut lumen (4). Only the microbes that can by-pass innate defenses have the ability to infect and cause disease.

The epithelial and sub-epithelial region of mucosal surfaces contains abundant immunocytes of many varieties. Indeed, in a healthy human adult, the mucosal immune system contributes almost 80% of all immunocytes (5). The number of immunoglobulin (Ig)-secreting cells in this population exceeds by several fold the number of Ig-secreting cells in all other lymphoid organs (spleen, bone marrow, and lymph nodes) combined (6). Importantly, these cells also have the ability to directly sense danger through expression of surface receptors specific for conserved microbial products. Under the influence of signals from the epithelium, stimulation through these receptors induces these cells to secrete cytokines and other modulatory factors. These factors work in concert with the epithelial signals to alert and dictate adaptive responses (7). In this way, cooperation of leukocytes and epithelial cells extends the definition of the innate immune system to include all cells of the body (8).

Enteroendocrine cells (EEC) form the largest endocrine system in the body. They secrete multiple regulatory molecules which control physiological and homeostatic functions, particularly postprandial secretion and motility. Their key purpose is to act as sensors of luminal contents, either in a classical endocrine fashion, or by a paracrine effect on proximate cells, notably vagal afferent fibers (9). They also play a pivotal role in the control of food intake, and emerging data add roles in mucosal immunity and repair.

The primary responsibility for mucosal barrier function resides in the epithelial cell plasma membrane, which is impermeable to most hydrophilic solutes (in the absence of specific transporters). Accordingly, direct epithelial cell damage, such as that induced by mucosal irritants or cytotoxic agents, including surfactants and some drugs used for cancer chemotherapy, results in a marked loss of barrier function. However, in the presence of an intact epithelial cell layer, the paracellular pathway between cells must be sealed or

modulated in physiological conditions. This function is mediated by an apical junctional complex, formed by tight junction and adherents junctions (10; 11) (Figure 1).

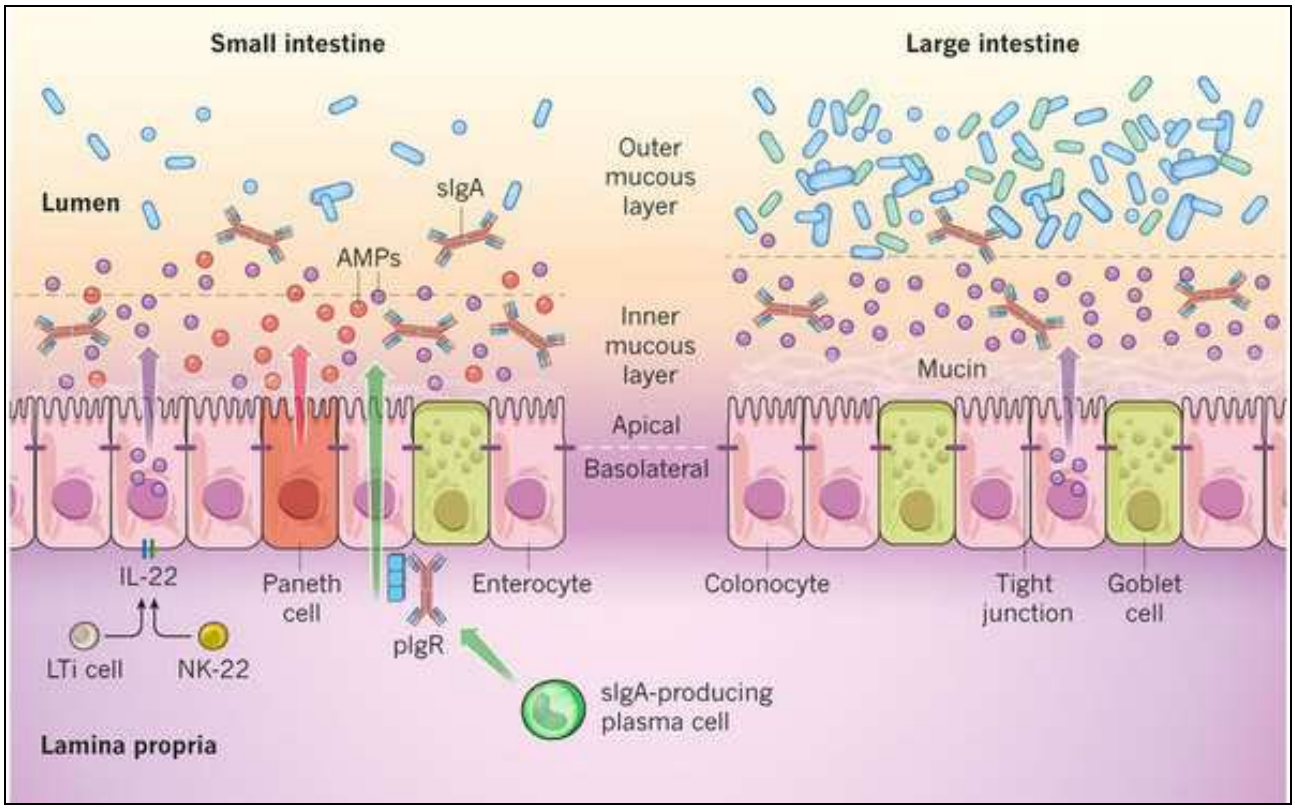

Figure 1: *Distinct subpopulations of IEC cells. IECs are integrated into a layer presenting two main regions, apical and basolateral. Enterocytes, in the small intestine, and colonocytes in the large intestine, as well as specialized Paneth cells in the bases of small intestinal crypts continually senses the microbiota to induce the production of antimicrobial peptides (AMPs). Goblet cells produce mucus, organized into a dense gel that forms an IEC-adherent inner mucous layer, and a less dense outer mucous layer. The outer layer is highly colonized by constituents of the microbiota. The inner mucous layer is largely impervious to bacterial colonization or penetration due to its high concentration of bactericidal AMPs.*

Junctional systems complexes are key players of the epithelial barrier effect

The elements of the complexes, identified as zonula occludens (tight junction), zonula adhaerens (intermediary junction), and macula adherens (desmosome), occupy a juxtaluminal position and succeed each other in the order given in an apical-basal direction.

The zonula occludens (tight junction) is characterized by fusion of the adjacent cell membranes resulting in closure of the intercellular space at variable distances. Within the

closed region, the dense outer leaflets of the adjoining cell membranes converge to form a single intermediate line. A diffuse layer of dense cytoplasmic material is often associated with this junction and its development varies from one epithelium to another.

The zonula adhaerens (intermediate junction) is characterized by the presence of an intercellular space (~200 Å) occupied by homogeneous, apparently amorphous material of low density; by strict parallelism of the adjoining cell membranes over distances of 0.2 to 0.5 µm; and by conspicuous bands of dense material located in the subjacent cytoplasmic matrix.

The desmosome or macula adhaerens is also characterized by the presence of an intercellular space (~240 Å) which, in this case, contains a central disc of dense material; by discrete cytoplasmic plaques disposed parallel to the inner leaflet of each cell membrane; and by the presence of bundles of cytoplasmic fibrils converging on the plaques (12-14) (Figure 2).

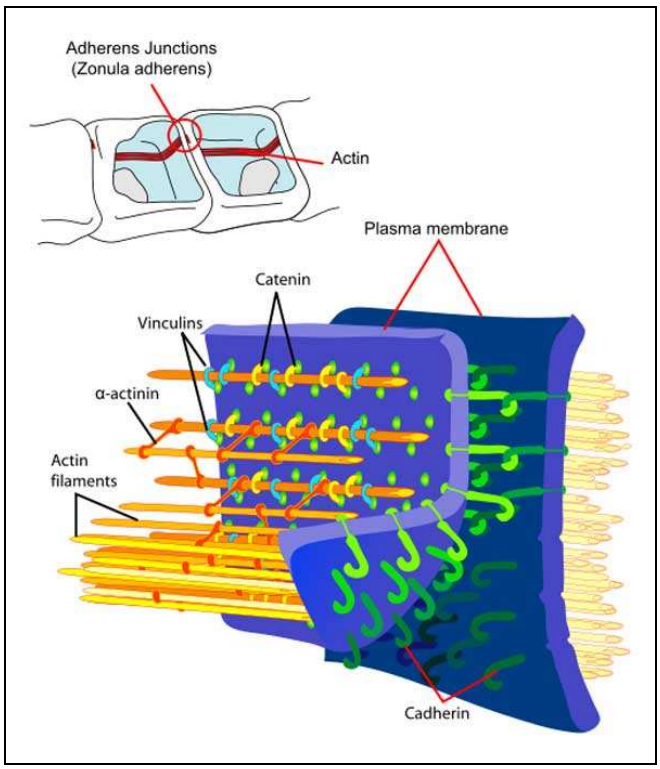

Figure 2: *scheme of adherens junctions main components*

Tight junctions are multi-protein complexes composed of transmembrane proteins, peripheral membrane (scaffolding) proteins and regulatory molecules including kinases (Figure 3).

Tight junctions limit solute flux along the paracellular pathway, which is typically more permeable than the transcellular pathway. Tight junctions have also the role of rate-limiting step in transepithelial transport and are the principal determinant of mucosal permeability. Thus, it is important to understand the specific barrier properties of the tight junction, which can be defined in terms of size selectivity and charge selectivity.

A second pathway is characterized by small pores that are thought to be defined by tight junction-associated claudin proteins, which are also primary determinants of charge selectivity. These pores have a radius that excludes molecules larger than 4 Å.

The expression of claudins varies between organs and even within different regions of a single organ and, as detailed below, can be modified by external stimuli, such as cytokines. Thus, tight junctions show both size selectivity and charge selectivity, and these properties may be regulated individually or jointly by physiological or pathophysiological stimuli.

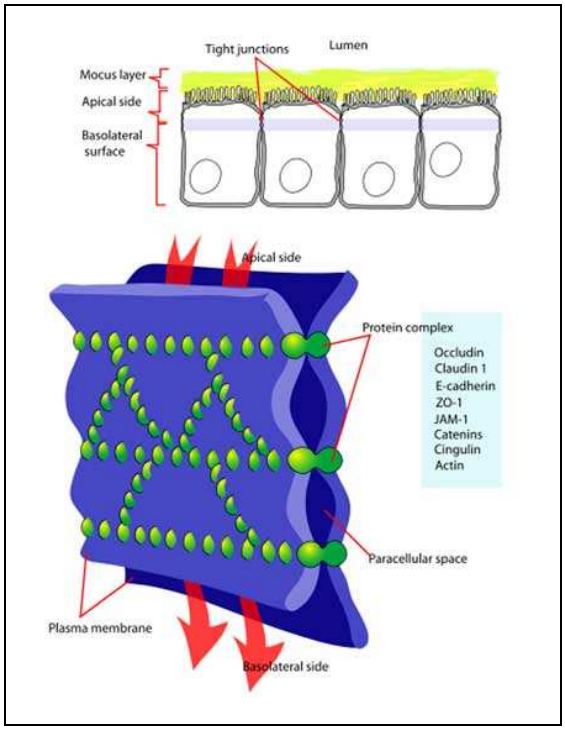

Figure 3: *Tight Junctions structure and mayor components*

At present, the most well-studied tight junction proteins are the claudins, a large family that includes at least 24 members (15-16). These proteins have four transmembrane helices with a very short intracellular amino-terminal sequence and a somewhat longer C-terminal tail. The first extracellular loop is approximately 50 residues long, although there is some variation among claudin family members. More importantly, sequence variation within the first extracellular loop determines tight junction charge selectivity (17), consistent with the view that the array of claudin proteins expressed in a given cell type defines the paracellular pore (18; 19) through which ions and perhaps nonionic solutes travel. The second extracellular loop of claudins is smaller than the first, ranges from 16 to 33 amino acids in length, and is poorly characterized. The cytoplasmic C-terminal tail varies in length from 21 to 63 residues and is the least conserved region of claudin proteins, suggesting that the tail may also be a site of functional regulation. Importantly, almost all claudin proteins present a three-aminoacid terminal motif that binds to PDZ domains (Figure 4). Tight junction proteins panel include ZO-1 as well as the related proteins ZO-2 and ZO-3 (20); each of these proteins contains three PDZ domains within the amino-terminal portion

of the protein. PDZ domains, which were initially identified in PSD95, DlgA, and ZO-1, are specialized for protein interactions. In the case of ZO-1, ZO-2, and ZO-3, the most aminoterminal PDZ domain binds to the C-terminal tail of claudins (21). This is functionally critical because deletion of the PDZ-binding motif prevents efficient claudin targeting to the tight junction. Moreover, ZO-1 and ZO-2 are each able to direct claudins to developing tight junctions (22); simultaneous elimination of ZO-1 and ZO-2 expression blocks claudin recruitment and tight junction formation with consequent lost of barrier function (23).

Several other groups of proteins, including transmembrane, cytoskeletal, and signaling proteins (24) complete the tight junction complex; in particular actin and myosin are essential structural elements of the tight junction (25).

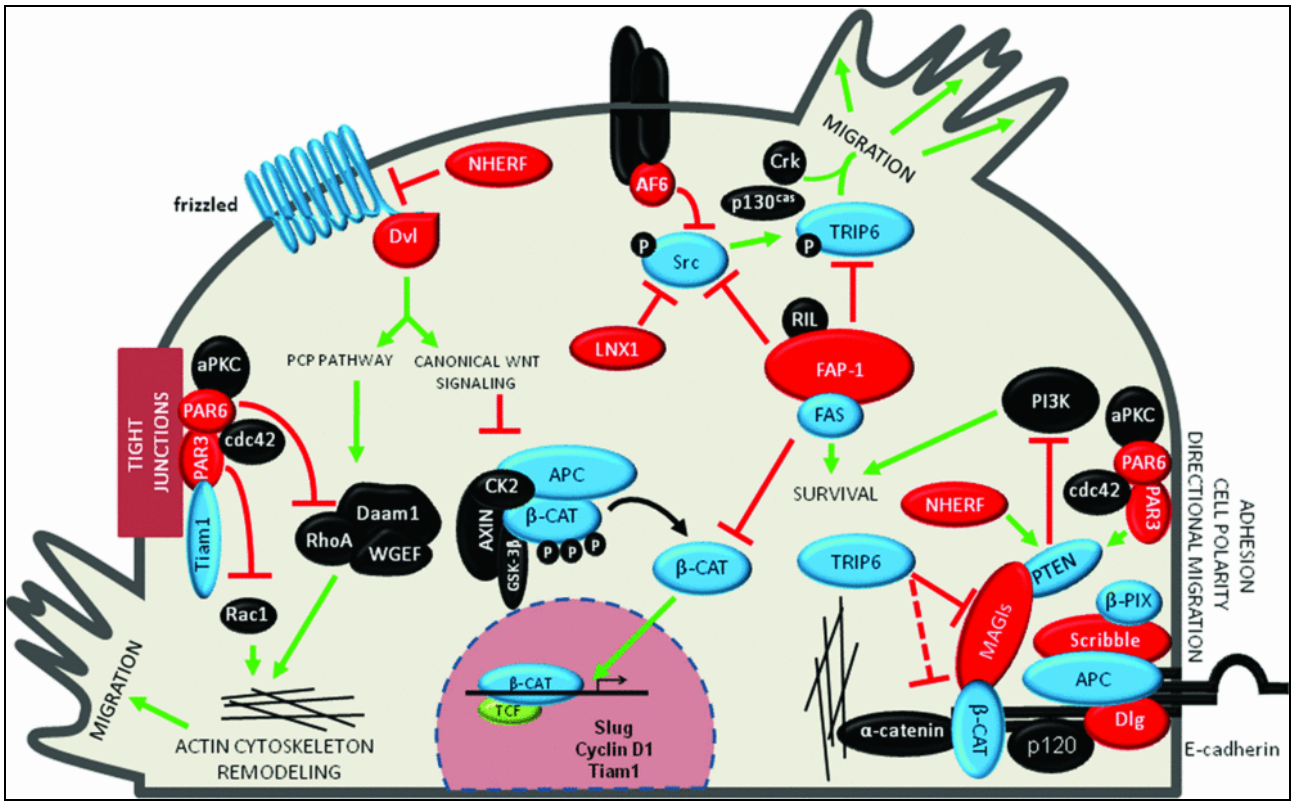

Figure 4: *PDZ domain interactions and the regulation of EMT and Wnt signalling. Schematic diagram of some of the critical regulators involved in the regulation of the canonical and non-canonical Wnt signalling pathways. Interlinked with this are PDZ interactions important in the regulation of EMT. Proteins possessing PDZ domains are shown in red and those possessing PBMs are shown in blue. β-CAT, β-catenin; CK2, casein kinase 2; GSK-3β, glycogen synthase kinase 3β; PCP, planar cell polarity; TCF, T-cell factor; WGEF, weak-similarity GEF.*

The best-characterized example of tight junctions regulation in response to physiological stimuli is represented by the reversible increase in intestinal paracellular permeability induced by apical $Na^{+/}$nutrient co-transport (26; 27); increase in paracellular permeability is thought to allow passive paracellular flux of nutrients, along with water. Ultrastructural analyses of tight junctions showed that activation of Na^{+}/nutrient co-transport induced condensation of perijunctional microfilaments (28), interpreted as an indicator of actomyosin contraction. Unfortunately no tools needed to study these biochemical events in intact tissue are still developed. To solve problem, an *in vitro* model that simulate Na^{+}/glucose co-transport–induced tight junction regulation was developed through use of cultured intestinal epithelial cell monolayers (29). Based on the ultrastructural data, phosphorylation of myosin II regulatory light chain (MLC), a trigger for actomyosin contraction, was examined and shown to increase following activation of Na^{+}/glucose co-transport (30). Moreover, MLC-kinase (MLCK) inhibition prevented both MLC-phosphorylation and barrier regulation induced by Na^{+}/glucose co-transport in cultured monolayers and also blocked barrier regulation in intact intestinal mucosa (31). These data suggest that MLCK is a critical physiological regulator of tight junction permeability. Furthermore, in vitro studies of epithelial cells with inducible expression of constitutively active MLCK demonstrate that enzymatic MLCK activation is sufficient to trigger downstream events necessary for barrier regulation (32).

Immune stimulation and barrier regulation: the fundamental role of apoptotic signals

The ability of cytokines, such as TNF and IFNγ, to regulate the function of the tight junction (33) barrier was first described 20 years ago. Since then, increased tight junction protein transcription, vesicular removal of proteins from the tight junction, tight junction protein degradation, kinase activation and cytoskeletal modulation have all been proposed to mediate cytokine-induced loss of tight junction barrier function (34). Although extensive

apoptosis of epithelial cells may also cause barrier loss, the relevance of single-cell apoptosis to barrier dysfunction remains controversial owing to differing results in diverse experimental systems.

TNF and IFNγ modify tight junction barrier function in intestinal, renal, pulmonary and salivary gland epithelia as well as between endothelial cells. The effects of TNF on barrier integrity have been best studied in the gut (35), where this cytokine has a central role in many diseases associated with intestinal epithelial barrier dysfunction, including inflammatory bowel disease, intestinal ischaemia and graft-versus host disease. For example, although the effect of therapy with TNF-specific antibodies may be largely due to the overall reduction in inflammation. Increased mucosal TNF production may also contribute to increased intestinal permeability and susceptibility to colitis in mice with defective mucin biosynthesis. MLCK has been shown to have a central role in TNF induced epithelial and endothelial barrier deregulation, both *in vitro* and *in vivo* (36). Similar to Na^+/nutrients co-transport, TNF-induced MLCK activation seems to increase paracellular flux through the leak pathway. Similarly, MLCK expression and activity are increased in intestinal epithelial cells of patients with inflammatory bowel disease.

1.2 BARRIER BREAKDOWN: THE PANDORA'S BOX OPENED

Chemotherapy-induced gastrointestinal mucositis

Many anti-cancer therapeutic strategies based on radiotherapy and chemotherapy are effective in the treatment of malignant disease but, conversely, present a plethora of side effects including oral and gastrointestinal mucositis. There is no approved therapy to prevent or treat chemotherapy-induced mucositis at present and the development of an effective intervention is seen as a high priority in oncological supportive care (37-39).

Severe mucositis is especially common among patients who receive aggressive myeloablative chemotherapy and in patients who receive radiation therapy as treatment for cancers of the oral cavity, oropharynx, nasopharynx and salivary glands. Patients with

severe mucositis develop ulcerations that penetrate fully into the submucosa and cause severe pain, which routinely necessitates narcotic analgesia.

In addition to the symptoms of mucositis and its impact on quality of life, mucositis adversely affects a variety of other health and economic outcomes. Among patients who have received chemotherapic treatments, the presence of mucositis results in lengthened hospital stays, increased use of resources and higher costs. Mucositis also threatens the efficacy of treatment plans by necessitating breaks in chemotherapy, reductions in doses of drugs used in chemotherapy and modifications in the selection of anti-neoplastic agents. Anthracyclines like doxorubicin are among the most widely used and effective chemotherapeutic agents but also the use of which often causes the onset of mucositis (especially in combination with 5-fluorouracil) (40-42).

One of the most important event that compromise the intestinal epithelium biological functions (like nutrients absorptions and barrier effect against pathogens invasion) is the lack of the correct permeability caused by alterations of the junctional systems (43; 44) of epithelial cells in response to apoptotic events promoted by chemotherapeutic agents, events like apoptosis and inflammation, which affect the tunica mucosa, the vascular endothelium and the whole body, contribute to the onset of mucositis. One of the most important apoptotic pathways involves caspases; in particular caspase-3 that is connected with junctional damages; two target proteins for Tight Junctions and Adherent Junctions, zonula occludens-1 (ZO-1) and beta-catenin respectively, are down-regulated in presence of chemotherapy-induced apoptosis. (45; 46) Because the gastrointestinal tract present a vast array of microorganisms, loss of epithelial integrity, especially when patients undergo myeloablation, markedly increases the risk of bacteraemia, fungaemia and sepsis (47; 48)

Inflammatory Bowel Diseases (IBD)

Idiopathic IBDs such as Crohn disease and ulcerative colitis occur in clinically immunocompetent individuals whose characteristic symptoms and signs arise from a

robust, cytokine-driven (yet noninfectious) inflammation of the gut (49). Crohn disease is associated with excess IL-12/IL-23 and IFN-γ/IL-17 production that affects the small bowel and colon with discontinuous ulceration and full thickness bowel wall inflammation often including granulomas. Patients report gastrointestinal symptoms of abdominal pain, diarrhea, and rectal bleeding as well as systemic symptoms of weight loss, fever, and fatigue. Crohn disease patients can also develop obstructing structures of the bowel and inflammatory connections (fistulae) (Figure 5) between segments of bowel or between the bowel and skin and other organs. In comparison, ulcerative colitis is associated with excess IL-13 production, primarily affecting the colon, with a continuous inflammation of the mucosa nearly always involving the rectum and extending proximally (50).

It has been proposed that three main features should be present for IBD to occur: a genetically susceptible mucosal immune system; an antigen, or pro-inflammatory compound, which reaches the gut and can trigger the susceptible immune system; and an alteration in gut barrier function which allows antigens to have contact with the mucosal immune system (51).

Since the studies about Crohn's disease have shown immunological factors underlying onset of this disease, the conventional treatments for IBD as corticosteroids, mesalamine, and immunosuppressants, provide mostly to block downstream inflammatory events. Medical therapy relies on classic anti-inflammatory and immunosuppressant drugs: corticosteroids, mesalamine compounds, azathioprine, and derivatives of the latter. (52-54). Newer biological drugs such as anti–TNF-α antibodies targeting the general inflammatory cytokine, TNF-α, have added greatly to our ability to control IBD, but even this therapy is limited by lack or loss of efficacy and associated toxicities (55). Emerging therapies for IBD are focusing on major effector cytokines as they are identified in ongoing investigations, for instance using an anti–IL-12p40 antibody to neutralize the effects of IL-12 and IL-23 in Crohn disease (56).

Increased paracellular permeability was reported in patients with Crohn’s disease (CD) over 25 years ago (57). Although such barrier loss may be caused by erosions that occur in active disease, some approaches used to measure permeability partially excluded this possibility by normalizing absorption of the inert sugar lactulose to that of the smaller, and more easily absorbed, inert sugar mannitol (58) .

In recent years, several lines of evidence suggested that an increased intestinal permeability play a central role in the pathogenesis of IBD. In different animal models of Crohn's disease, an increased small intestinal permeability has been shown, even before disease expression, and the reversal of this barrier defect can attenuate the disease, implying that the increased permeability is not simply an epiphenomenon but rather is an important etiological event (59-61). In the human condition it is also evident that increased small intestinal permeability is commonly observed in populations at high risk of developing Crohn's disease (62; 63). This would suggest that there is a subtle alteration of function, independent of inflammation, which can be visible as an increase in paracellular permeability. This raises the possibility that restoration of barrier function may be therapeutic in CD Consistent with this hypothesis, emerging data indicate that inhibition of cytoskeletally mediated barrier dysfunction may be able to prevent disease progression. Barrier restoration may, therefore, represent a non-immunosuppressive approach to achieving or maintain disease remission.

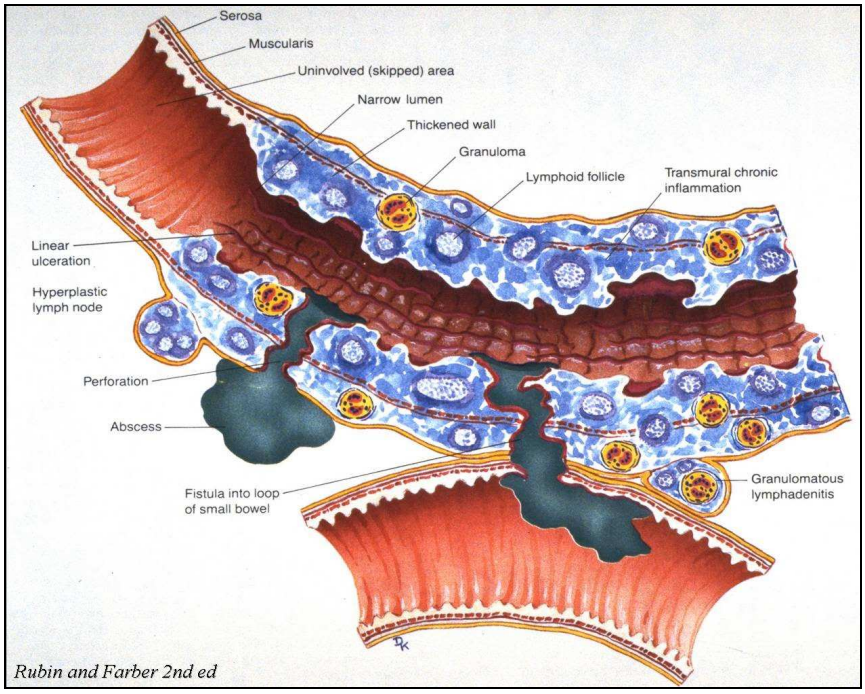

Figure 5: *Classical representation of Crohn Disease lesions*

1.3 SODIUM-DEPENDENT GLUCOSE TRANSPORTER-1

SGLT1: classical transporter and novel receptor. Two faces of the same medal

The primary functions of the gastrointestinal (GI) tract have traditionally been perceived to be limited to the digestion and absorption of nutrients and electrolytes and to water homeostasis but the intestinal epithelial barrier also controls the equilibrium between tolerance and immunity to non-self-antigens by regulating antigen trafficking both through the transcellular and paracellular pathways.

Luminal content influences intestinal epithelium function and the components of diet certainly play a role in the modulation of enterocytes response. The large surface of the gut is a wide area to protect and constitutes an easy way to the whole organism for pathogen bacteria. On the other hand a so large line on external environment is necessary to an appropriate absorption of the nutrients. Often the absorption is a transport against gradient because the concentration of nutrient molecules is lower in the lumen than inside the cells. For this reason a wide range of transporters are evolved in order to guarantee

the absorption of water and electrolytes, minerals and vitamins, sugars, fatty acids, amino-acids and small peptides. The same molecules probably exert different effects on the role of IECs in mucosal immunity. D-glucose, in particular, is prevalently considered as energetic substrate and other possible roles are poorly analyzed.

Glucose is among the more abundant monosaccharide in the diet, and its absorption in the intestine is mediated by the high-affinity, sodium-dependent glucose cotransporter (SGLT-1), located in the apical membrane of enterocytes.

Recently SGLT-1 has been described as involved in the repair of plasma membrane integrity and tight junction (TJ) integrity injured by heat stress or cisplatin chemo-treatment (45; 64) In our recent papers we demonstrate the protective effect of the activation of sodium-dependent glucose transporter-1 (SGLT-1) on damages induced by TLRs ligands in intestinal epithelial cells, in a murine model of septic shock and in LPS-induced liver injury, as well as liver injury and death induced by an overdose of acetaminophen (65; 66).

Intestinal glucose absorption and the role of SGLT-1

D-glucose is the major source of energy in mammals and it is absorbed by the epithelial cells lining the surface of the small intestine. The transport of glucose from lumen to enterocytes in the small intestine is principally mediated by Na^+-dependent glucose co-transporters (SGLTs, members of a larger family of Na^+-dependent transporters, gene name SLC5A) that use the Na+-electrochemical gradient at the generated by the Na^+/K^+-ATPase to transport glucose into cells (Figure 6)

SGLT-1 is the most important active glucose transporter at intestinal level and it is found in brush border membrane of mature enterocytes in the small intestine. During the process of intestinal sugar transport, on the luminal side of the brush border membrane, two Na^+ ions bind to SGLT-1 and produce a conformational change that permits sugar binding. Another conformational change allows the substrates to enter the enterocyte. The sugar, followed by the Na^+, dissociates from SGLT-1 because the affinity of the cytosolic sites is low, and

also because the intracellular concentration of Na^+ is low (10 *vs* 140 mEq/L). The Na^+/K^+-ATPase in the basolateral membrane is responsible for maintaining the Na^+ and K^+ electrochemical gradients across the cell membrane (67-70).

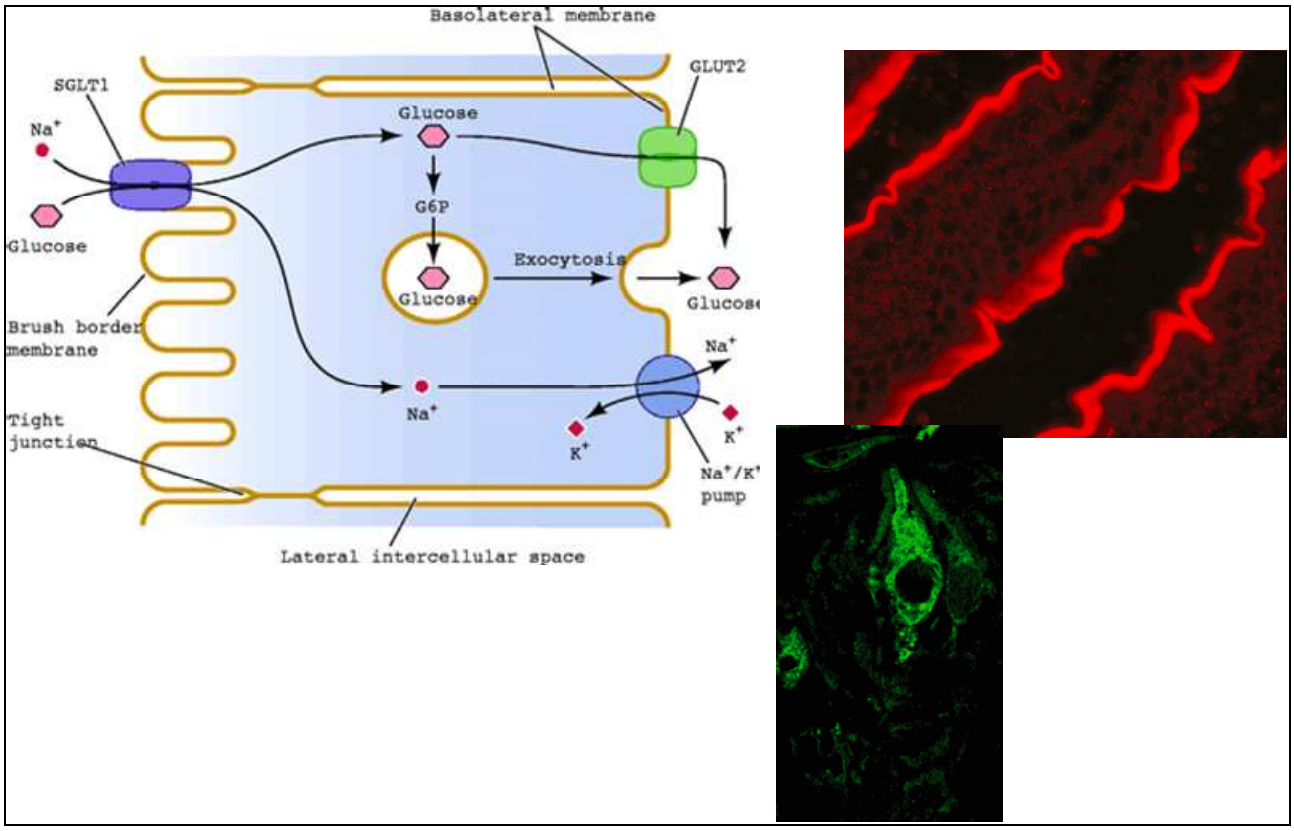

Figure 6: *schematic model of intestinal sugar transport. SGLT1 is the sodium dependent glucose/galactose transporter on the brush border membrane. The Na+K+-ATPase on the basolateral membrane maintains the gradient necessary for the functioning of SGLT1. GLUT2 transports glucose, galactose and fructose out of the cell. IF images of SGLT-1 in villus brush border.*

SGLT-1 as a new player in epithelial homoeostasis maintenance. Engagement with natural and synthetic molecules.

Since 2005 SGLT-1 assumes a novel physiological role. SGLT-1 activation loads to a local and systemic anti-inflammatory and cytoprotective response in different inflammatory conditions. Firstly the effect of glucose has been analysed in enterocytes exposed to agonists of TLR4 and TLR9. The encouraging in vitro results prompted us to analyze the effects of glucose on a systemic inflammatory response syndrome (endotoxic shock) in mice (Figure 7).

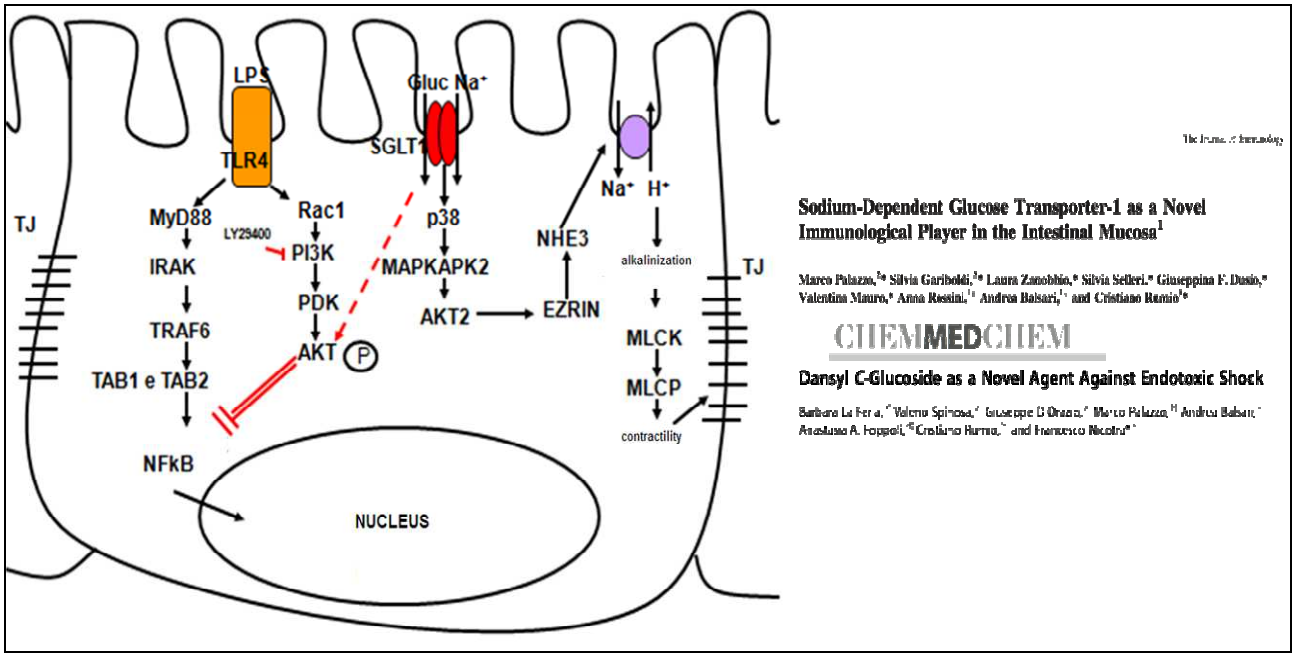

Figure 7: *schematic representation of SGLT-1 activation pathways in different cases of tissue damage*

Oral ingestion of glucose was found to protect 100% of mice from lethal endotoxic shock induced by intraperitoneal LPS administration (65); protection was only observed when glucose was administered orally, not by i.p. route, suggesting the important role of intestinal epithelial cells. Subsequently the study investigated the possibility that orally administered D-glucose exerts a systemic anti-inflammatory activity on hepatic liver failure. In this study (66) that D-glucose prevents LPS-induced liver injury, as well as liver injury and death induced by acetaminophen overdosing. In both of these models, physiological liver morphology is maintained and organ protection was confirmed also by unchanged levels of circulating markers of hepatotoxicity, such as ALT or LDH. In addition, D-glucose was found to protect liver from alpha-amanitin intoxication. In this case, however, a second signal had to be present in addition to glucose in order to achieve protective efficacy.

In addition, we observed that the *in vivo* protection depends from a systemic increase of anti-inflammatory cytokine IL- 10. The milestone of the observed immunomodulatory effects resides in activation of SGLT-1; in fact, the glucose analogue 3-OMG, which induces the transporter activity but is not metabolized, exerted the same effects as glucose both in vitro and in vivo. Unfortunately 3-OMG is active at the same high concentration of

D-glucose and in order to solve this problem we decided to screen a library of synthetic glucose analogues as ligands for our experiments.

BLF501: origin of the synthetic compound

In the search for non-metabolizable glucoderivatives able to "activate" the SGLT-1 transporter at pharmacological concentrations, the chemical researcher team generated a small library of naphthyl *C*-glycoside and glycitol derivatives, mostly without the use of protecting groups. We tested *in vitro* anti-inflammatory activity of different compounds, among them, we have selected a synthetic SGLT-1 ligand, named BLF501 (figure 8), which binds to the transporter with high potency, i.e. at concentrations 5 orders of magnitude lower than glucose.

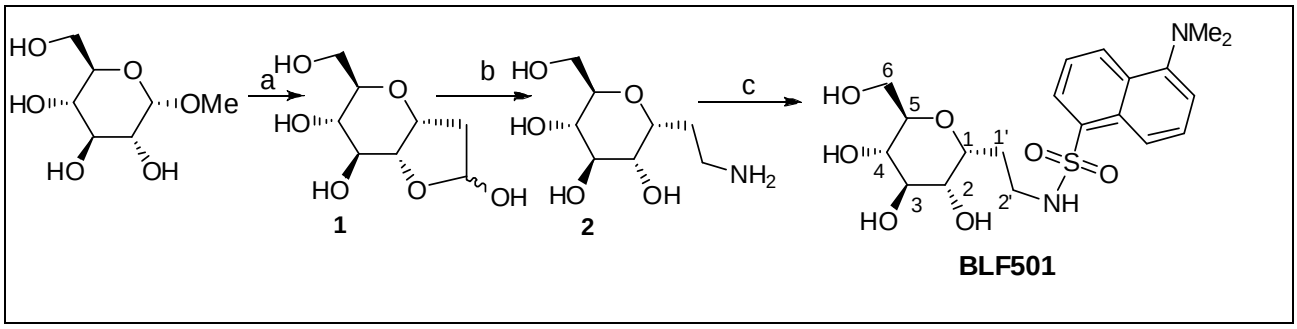

Figure 8: *Synthesis and Structure of BLF501*

BLF501, a member of the C-glycoside class, was designed to resist glucose metabolism and to retain hydrolytic stability in the acidic and basic conditions found in the gastrointestinal tract. Stability of BLF501 in different pH conditions was tested in samples prepared by dissolving 2.3 mg in 550 µl of D_2O and adjusting the pH to 1.2 through DCl addition (acidic conditions) or by dissolving 3 mg of BLF501 in 550 µl of D_2O and adjusting the pH to 12.5 through NaOD addition (basic conditions). Both samples were kept at room temperature until ^{1}H-NMR spectra were recorded at 10 min, 4.5 h and 24 h. As shown in Figure 2, neither sample evidenced degradation in 24 h. BLF501 matches with the fundamental characteristic of absence of metabolic activity. In fact in the field of C-glycosides like BLF501 no relevant bioactivity has been reported until now (71), allowing us to consider BLF501 a non-metabolizable glucose derivate.

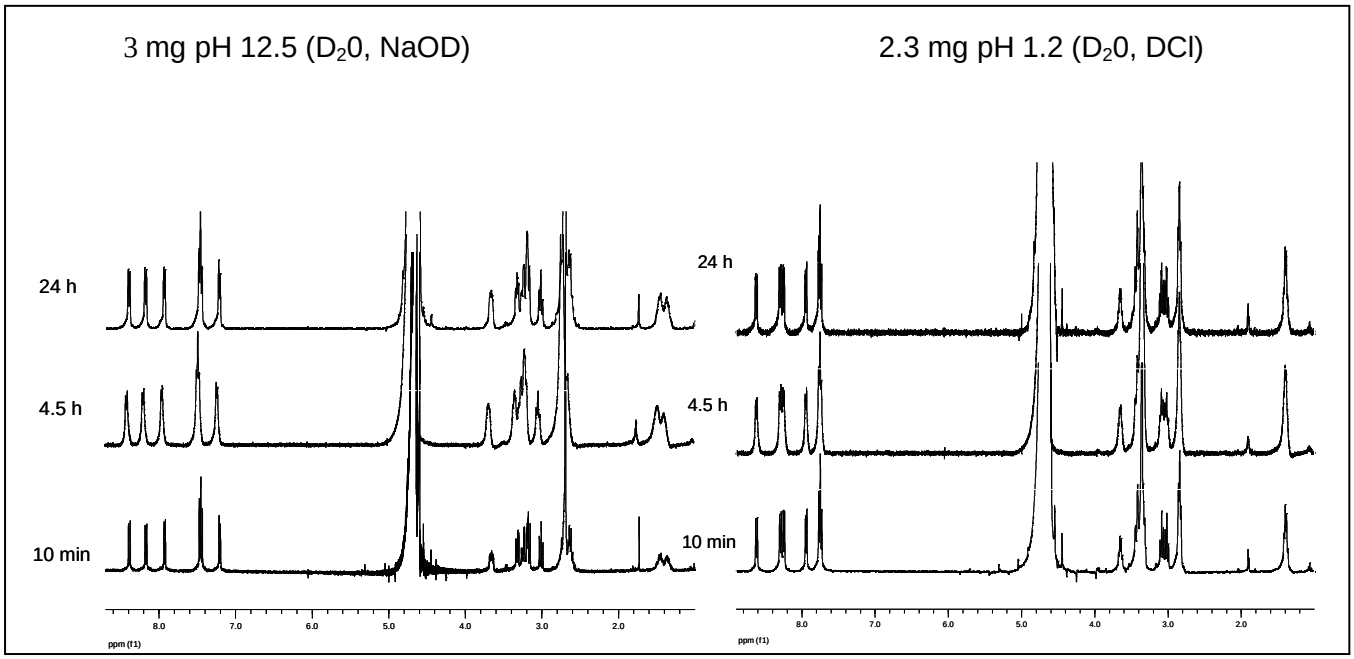

Figure 9. *^{1}H-NMR spectra of BLF501 at pH 12.5 and at pH 1.2.*

1.4 AIM OF THE STUDY:

The aim of this work is to demonstrate that SGLT-1 engagement *via* orally administered ligands, in particular the synthetic one BLF501, could activate protective mechanisms at intestinal epithelial level, preserving correct epithelial morphology and permeability and accelerating recovery of homeostatic conditions.

2. MATERIALS AND METHODS:

2.1 SGLT-1 ACTIVATION IN GIM MODELS:

Chronic and acute *in vivo* experiments were performed on mice strain BALB/C purchased from Charles River Italy. The mice used for the different treatments were housed in specific aseptic conditions, with a constant temperature and humidity and received food and water ad libitum. The animals were divided randomly into groups and assigned to two treatment protocols.

Chronic treatment:

15 animals formed the control group; 15 animals formed the group treated with doxorubicin and 5-fluorouracil, 15 animals formed the group treated with doxorubicin and 5-fluorouracil and BLF501 25 µg/Kg; 15 animals formed the group treated with doxorubicin and 5-fluorouracil and BLF501 2.5 µg/Kg; 15 animals formed the group treated with doxorubicin and 5-fluorouracil and BLF501 0.25 µg/Kg and 15 animals formed the group treated with BLF501 25 µg/Kg only. Administration of doxorubicin (DXR) 7 mg/kg (adriablastina, Pfizer) and 5-fluorouracil (5-FU) 100 ng / kg (fluorouracil; TEVA), dissolved in saline solution for a final volume of 300 µl, was carried out weekly for a total duration of three weeks by intraperitoneal injection. The administration of BLF501 (25, 2.5 and 0.25 µg/kg in saline for 100µl total) occurred simultaneously with the chemotherapic agents by gavage using a gastric tube.

Acute treatment:

Administration of DXR (20 mg/kg), dissolved in saline solution for a final volume of 300 µl, was carried out at day 0 intraperitoneal injection. The administration of BLF501 (25 µg/kg in saline for 100 µl total) occurred simultaneously with the chemotherapic agent by gavage using a gastric tube

7 animals formed the control group; 14 animals formed the group treated with DXR; 14 animals formed the group treated with DXR and BLF501; 14 animals formed the group

treated with BLF501. Seven mice from all treated groups were sacrificed after 48 and 72h. Control group was sacrificed after 72h. All the animals of acute treatment received, an hour prior to sacrifice, an intraperitoneal injection of bromodeoxyuridine (BrdU) to perform evaluation of cell proliferation with immunofluorescence reaction.

Chemotherapy simulation:

Chemotherapy simulation *in vivo* experiments was performed on mice strain SKH-1 nude mice purchased from Charles River Italy. The mice used for the different treatments were housed in specific aseptic conditions, with a constant temperature and humidity and received food and water ad libitum. A431 tumoral cells were implanted subcutaneously to 32 mice and when the tumor weight reached a mean value of 240 mg mice were divided randomly into groups and assigned to the treatment protocols. 8 animals formed the control group; 8 animals formed the group treated with doxorubicin 6 mg/Kg 8 animals formed the group treated with doxorubicin 6 mg/Kg plus BLF501 25 µg/Kg; 8 animals formed the group treated with BLF501 25 µg/Kg only. Tumor weight was registered daily. At day 26 of treatment mice were sacrificed.

Processing of samples

After collection, the samples were fast separated in small pieces and fixed in 10% formalin with 2% sucrose for 4 hours at 4 °C. Then we proceeded with 2 rinses in PBS half-hour after each and were placed in 70% ethanol for at least 12 hours, finally the samples were dehydrated by successive steps in an ascending scale of alcohols, placed in xylene for 2 hours and finally embedded in paraffin.

Staining with hematoxylin and eosin

Hematoxylin-eosin staining was performed on sections obtained from paraffin-embedded samples. The samples were deparaffinized in xylene, rehydrated through descending scale of alcohol, left for 10 minutes in hematoxylin, washed under running water and then placed in eosin for 3 minutes, finally dehydrated through ascending scale of alcohols and

xylene in then mounted with coverslips using Entellan (Merck, Darmstadt, Germany). The observation of the samples and photographs were taken with a microscope Nikon Eclipse 80 with a digital camera Nikon DS-L1.

ZO-1 Immunofluorescence

Samples sections were deparaffinized in oven at 60 °C for 30 minutes, placed in xylene and rehydrated. It was then performed a quick rinse with 0.1 M Tris/HCl pH 7.4 after which the sections were incubated with proteinase K 20 g/ml Tris/EDTA buffer pH 8 for 15 minutes at 37 °C. It was subsequently made a furth er washing with Tris/HCl after the sections were permeabilized with 1% Triton X-100 in Tris/HCl for 5 minutes at room temperature. Slides were washed with Tris/HCl and then sections were blocked with a solution containing 1mM Hepes, 2% goat serum, 1x HBSS and 0.5% Triton X-100 for one hour at room temperature. Sections were incubated with primary antibody α-ZO-1 (Invitrogen, Camarillo, CA) 1 5 g / ml in Tris/HCl overnight at 4 °C. Samples were washed for three times with Tris/HCl and 0.01% Triton X-100. After washing, the sections were incubated with secondary antibody goat anti-rabbit conjugated to tetramethyl-rhodamine isothiocyanate (TRITC) diluted 1:1000 in Tris/HCl for 45 minutes at room temperature.

We proceeded with further washes for 5 minutes with Tris/HCl + 0.01% Triton X-100, then the sections were incubated with 20µl of enhancer per slice for 30 minutes at room temperature. 2 more washes were carried out for 5 minutes with Tris/HCl and 0.01% Triton X-100. Sections were incubated with DAPI 1:10000 in Tris/HCl for 5 minutes at room temperature and then subjected to 3 washes with Tris/HCl and 0.01% Triton X-100. Slides were mounted with Mowiol. The observation of the samples and photographs were taken with a microscope Nikon Eclipse 80, with a digital camera Nikon DS-L1.

Beta-catenin immunohistochemistry.

The sections on slides were deparaffinized in oven at 60 °C for 30 minutes, placed in xylene and rehydrated It was then performed using two antigen unmasking steps

interspersed with 5 minutes 1 minute pause, in a microwave oven with citrate buffer pH 6 = 0.005 M. The sections were cooled for about an 30 minutes and then washed with 0.1 M Tris/HCl pH 7.4 + 0.025% Triton X-100 (three washes of 5 minutes each). Then was carried out the endogenous peroxidase inhibition with a solution of 3% H_2O_2 in 0.1 M Tris/HCl pH 7.4 for 20 minutes, after which the sections were washed with 0.1 M Tris/HCl pH 7.4 + 0.025% Triton X- 100 (three washes of 5 minutes each). Subsequently nonspecific sites were blocked with HHG solution (1 mM Hepes, 2% goat serum, 1X HBSS, 0.5% Triton X-100) in Tris/HCl for 1 hour at RT. Sections were incubated with primary antibody anti-beta-catenin (Abcam, Cambridge, UK) 1:500 in Tris/HCl + 1% BSA for 2 hours at RT, followed by 3 washes for 5 minutes with Tris/HCl, 0.1% Triton X-100. After washing, the sections were incubated with biotinylated secondary antibody goat anti-rabbit 1:1000 diluted in 0.1 M Tris/HCl pH 7.4 + 0.025% Triton X-100 for 45 minutes at room temperature. After washes with 0.1 M Tris/HCl pH 7.4 + 0.025% Triton X-100 sections were incubated with ABC-kit and DAB (Vector, Burlingame, U.S.), the development has been blocked in distilled H_2O. Sections were counterstained with hematoxylin for 10 minutes RT and finally dehydrated through ascending scale of alcohols and xylene, then mounted with coverslips using Entellan (Merck, Darmstadt, Germany). The observation of the samples and photographs were taken with a microscope Nikon Eclipse 80th, with a digital camera Nikon DS-L1.

Immunofluorescence for BrdU

The sections on slides are deparaffinized in oven at 60 ° C for 30 minutes, placed in xylene and rehydrated sections were rinsed in PBS and incubated with 2N HCl for 30 minutes at RT and in $Na_2B_4O_7$ for 1o minutes. Sections were incubated with PBS/3% BSA for 20 minutes at RT and then with proteinase K 20 g/ml in TrisEDTA buffer pH 8 for 15 minutes at 37℃. After three washes in PBS/BSA 3% s ections were incubated with primary antibody α-BrdU (Novocastra) 1:200 in PBS/3% BSA for 1 hour at RT, washed with

PBS/3% BSA and then incubated with secondary antibody goat anti- mouse Alexa Fluor 488 1:500 in PBS/BSA 3%. Slides were washed with PBS/BSA 3% and with Tris/HCl/0.01% Triton X-100. Sections were incubated with 1:2500 DAPI in Tris/HCl for 5 minutes at room temperature and then subjected to 3 washes with PBS / BSA 3%. Slides were mounted with Mowiol.

Real-Time polymerase-chain reaction (PCR)

Real-Time PCR experiments were performed in accordance with manufacturer's instructions using a 7900HT Fast Real Time PCR System (Applied Biosystems, Foster City, CA, US). Primers for SI; TFF3; DLL1, and beta-actin were purchased from Applied Biosystems.

Western Blots

The expression of Akt/P-Akt, Caspase-3 and Ezrin was assessed by analyzing the total protein extract from small intestine samples taken from differently treated animals. The protein extracts were quantified using the BCA method (BCA Protein Assay Kit, Pierce, Rockford, IL). Proteins (30 µg) were fractionated on a polyacrylamide gel (BIO-RAD Labs, Hercules, CA) containing 0.1% to 8% of SDS and transferred onto a nitrocellulose filters (American Biosciences, Buckinghamshire, England) by electroblotting. Filters were incubated for 1 hour in TBS (8% NaCl, 3% Tris) containing 1% Tween-20 and 5% milk powder to block nonspecific binding sites. For the various reactions following antibodies were used:

Protein	**Primary Ab**	**Primary Ab dilution**	**Solvent solution**	**Reaction conditions**
Akt	monoclonal anti-mouse Akt	1:1000	TBS + 1% Tween-20 +5% milk	O/N at 4℃
P-Akt	monoclonal anti-mouse P-Akt	1:1000	TBS + 1% Tween-20 +5% milk	O/N at 4℃
Caspase-3	policlonal rabbit anti-mouse caspase-3	1:500	TBS	O/N at 4℃
Ezrin	monoclonal anti-mouse Ezrin	1:1000	TBS	O/N at 4℃
Beta-actin	policlonal rabbit anti-mouse beta-actin	1:1000	TBS + 1% Tween-20 +5% milk	O/N at 4℃

Table 1: *primary antibodies used to perform WB assays*

After three rinses with TBS containing 1% Tween-20, the filters were incubated for 1 hour at room temperature with secondary antibody: rabbit anti-peroxide (Vector Laboratories) diluted 1:1000 in TBS with Tween-20 to 0.1% and 5% milk. Following three rinses were performed with TBS containing 1% Tween-20 and a rinse in TBS. The bands were finally visualized using the ECL ™ Western Blotting Detection Reagents and plates by autoradiography (American Biosciences).

Cell cultures

Cell lines Caco-2/bbe and Caco-2/bbe permanently transfected with SGLT-1 (kind gift of Prof. Mark Donowitz, MD, Johns Hopkins University School of Medicine, Baltimore) were cultured in DMEM high-glucose medium (4,5g/L) (Euroclone, Pero, Italy) supplemented with 10% FBS (Euroclone), 1% glutamine (Euroclone), 15 nM sterile HEPES solution (Euroclone). For Caco-2/bbe/SGLT1 cells, 250 µg/ml G418 gentamicin bisulfate salt solution (Sigma-Aldrich) was added as antibiotic agent; for normal Caco-2/bbe penicillin/streptamicin solution (Euroclone) was added.

A431 cells were cultured in RPMI 1640 medium (Euroclone) supplemented with 10% FBS (Euroclone), 1% glutamine (Euroclone) and 1% penicillin/streptamicin solution (Euroclone).

Cell treatments

For viability assays 1 x 10^5 Caco-2 cells were plated on 96 flat-bottom well plates and treated after 24 hours with doxorubicin (100 µM) with or without BLF501 11.4 µM. Cell viability was evaluated after 48 h with Neutral Red assay.

2.2 SGLT-1 ACTIVATION IN IBD MODELS

Mice and in vivo treatments

C57BL/6 female mice were purchased from Charles River, Italy (Head Office Wilmington, MA). Mice were housed under specific pathogen-free conditions, maintained at constant temperature and humidity, with food and water given ad libitum, and used at 8-12 weeks of age. Experimental protocols were approved by the Ethics Committee for Animal

Experimentation of Istituto Nazionale Tumori, Milano, and carried out according to guidelines of the United Kingdom Co-ordinating Committee on Cancer Research for animal welfare in experimental neoplasia (1998).

Induction of acute and chronic colitis

Mice weighting 20-22 g received 2% dextran sodium salt (m. m. 40 kD, MP Biomedicals, Irvine, CA) ad libitum in filter-purified drinking water for 7 days. For treatments studies mice undergoing DSS from day 4 at day 7 received oral administration of BLF501 250 µg/kg or 25 µg/kg or 2.5 µg/kg once day. BLF501 was administrated with a sterile gastric tube In other mice groups received only BLF501 250 µg/kg or 25 µg/kg or 2,5 µg/kg or glucose 2,5 g/kg. One group received only DSS 2% in drinking water.

Day 1	Day 2	Day 3	Day 4	Day 5	Day 6	Day 7	Day 8
DSS 2%	DSS 2%	DSS 2%	DSS 2% +BLF501	DSS 2% +BLF501	DSS 2% +BLF501	DSS 2% +BLF501	Sacrifice

Table 2*. Schematic presentation of different treatments in the time. Mice received DSS 2% in drinking water. BLF501 250 µg/kg or 25 µg/kg or 2,5 µg/kg were administrated (diluted in physiological solution) once per day at day 4, 5, 6, 7 and at 8th mice were sacrificed.*

Groups	**Treatment**
1	Untreated
2	DSS 2% only
3	DSS 2% + BLF501 250 µg/kg
4	DSS 2% + BLF501 25 µg/kg
5	DSS 2% + BLF501 2,5 µg/kg
6	BLF501 250 µg/kg
7	BLF501 25 µg/kg
8	DSS 2% + physiological solution

Table 3. *Schematic representation mice groups. 5 mice/groups.*

To induce chronic colitis four groups of 10 mice/groups mice received three cycles of DSS 2%. Each cycle consists of 2% DSS dissolved in filter-purified drinking water for 7 days, followed by a 14 days interval with normal water administration. After ten days from the last DSS cycle we started different treatments.

The first group of animals (control group) received normal drinking water only, during the whole time of the experiment. The second group of 12 mice received only three cycles of

treatment with DSS, as previously described, and no any further treatment. Four mice of this group were sacrificed one week after DSS cycle completion; four mice of this group were sacrificed two weeks after DSS cycle completion; and 4 mice were sacrificed after three weeks.

After DSS cycles completion, third mice group received oral administration of 25 µg/kg BLF501 four times/week for one week; forth received 25 µg/kg BLF501 four times/week for two consecutive weeks; and fifth group received 25 µg/kg BLF501 four times/week for three consecutive weeks.

Groups	**Treatments**
1	Untreated
2	DSS 2% +physiological solution
3	DSS 2%+ BLF501 25 µg/kg for 1 week
4	DSS 2% + BLF501 25 µg/kg for two week
5	DSS 2% + BLF501 25 µg/kg for three weeks

Table 4. *Schematic representation mice groups. 12 mice in group 1. In goups 2, 3, 4 and 5 10 mice/group.*

TREAT.	DSS	H_2O	DSS	H_2O	DSS	H_2O	BLF501 25 µg/kg	Death Group3/2	BLF501 25 µg/kg	Death Group4/2	BLF501 25 µg/kg	Death Group5/2
N days	7	14	7	14	7	10	7	X	7	X	7	X

Table 5 *Schematic presentation of different treatments time. N days is for number days of water DSS 2% added or water only administration. After ten days of the last DSS cycle BLF501 was orally administrated 4 times/week for 1 or 2 or 3 consecutive week. X is for sacrifice day.*

Evaluation of intestinal inflammation in acute and chronic colitis

Acute colitis was scored daily using standard parameters that includes evaluation of body weight and stool consistence. Body weight of mice was registered daily at 5.00 p.m.. Stool consistence was evaluated daily, but comparative analysis between different groups was conducted at the end of experiments.

Score	**Stool consistence**	**Blood**
0	Normal	No visibile
1	Soft but still formed	No visibile
2	Very soft	Blood traces in stool visible
3	Diarrea	Rectal bleeding

Table 6. *Scoring system for the comparative analysis of stool consistence.*

At the end of treatments the colon of mice was cut close to the ileo-cecal valve and rectum, and the length was measured with and .for acute colitis experiment photos were captured.

Ussing Chamber analysis..

In order to measure the colon permeability in 5 mice/group, organ segments were mounted between the two chambers of a Ussing System (0.125 cm^2 opening). Two calomel voltage-sensitive electrodes and two Ag-AgCl current passing electrodes (EVC-4000 World Precision Instrument Inc., Sarasota, FL) were connected to the Ussing chamber via agar bridges. Both the mucosal and serosal sides of the chamber were connected to sterilized circulating reservoirs containing 10 ml of oxygenated Krebs buffer (115 mM NaCl, 8 mM KCl, 1.25 mM $CaCl_2$, 1.2 mM $MgCl_2$, 2 mM KH_2PO_4, and 225 mM $NaHCO_3$; pH 7.35). The buffers were maintained at 37℃ by a heated water jacket and will circulate by a gas lift column of 95% oxygen/5% CO2. Glucose (5.5 mM) was added to the serosal and mucosal sides. Colonic membrane mounted in the Ussing chamber, the system was allowed to stabilize for 20 minutes, in order to test the system functionality and the integrity of the colonic mucosal membrane. Trans-epithelial electrical potential difference in millivolt across the mucosal membrane was measured directly, while the trans-membrane resistance was calculated indirectly as ohms x cm^2, using Ohm's law.

Histological evaluation of colitis severity.

Murine colon specimens of 5 mice/group will be fixed in 10% neutral buffered formalin, embedded in paraffin, sectioned at 4 μm and collected on xilanized slides. Histopathological analysis using hematoxylin-eosin-stained sections of distal colon samples of mice were performed. Samples were observed with a Nikon Eclipse 80i microscope equipped with a digital Nikon DS-L1 camera. To quantify/evaluate acute and chronic colitis-associated histological alteration in the colon we used a scoring system, provided in table 7.

Score	Histologic changes
0	No evidence of inflammation
1	Low level of inflammation with scattered infiltranting mononuclear cells
2	Moderate inflammation with multiple foci
3	High level of inflammation with increate vascular density and marked wall thickening
4	Maximal severity of inflammation with transmural leukocyte infiltration and loss of globet cells.

Table 7. *Scoring system for inflammation associated histological changes in the colon*

Immunofluorescence analysis.

Murine colon specimens were fixed in 10% neutral buffered formalin, embedded in paraffin, sectioned at 4 µm and collected on xilanized slides; samples were deparaffinized, rehydrated, and incubated for 10 minutes at 37 ℃ in a humidified chamber with protease type XIV 2 mg/ml (from Sigma) in Tris/HCl; samples were then incubated with glycine 0,1 M for 20 minutes at room temperature, washed with Tris/HCl + Triton X-100 0.01%, incubated with $NaBH_4$ 0.5mg/ml for 20 minutes at room temperature, washed with Tris/HCl + Triton X-100 0.01%, incubated with Image-IT FX signal enhancer (Invitrogen) for 30 minutes, blocked with 2% goat serum for 20 minutes at room temperature and incubated with rabbit anti-occludin or anti-ZO-1 antibody 4 µg/ml (both from Invitrogen). Incubation with secondary antibody 546 Alexa conjugated goat anti-rabbit and staining of the nuclei with DAPI were performer. Samples were observed with a Nikon Eclipse 80i microscope equipped with a digital Nikon DS-L1 camera.

3 RESULTS

3.1 SGLT-1 activation exerted by BLF501 accelerates recovery from the alterations of the small intestine induced by a single administration of DXR.

The effect of BLF501 on alterations of the small intestine induced by DXR was evaluated in mice treated with DXR alone (20mg/kg i.p., n=14); DXR plus BLF501 (25ug/kg BLF501 n=12); BLF501 alone (n=14) or left untreated (n=7). Half of the mice were sacrificed after 48 hours and the others after 72 hours.

Macroscopic examination of small intestine samples collected at 48 or 72 hours did not reveal morphological alterations. On the other hand, determination of the proliferation rate of crypt cells rate, performed by immunofluorescence BrdU assay, revealed a significant reduction of proliferation in DXR-treated mice (1.3 ± 0.2 % at 48 h; 0.8 ± 0.6 % at 72h, untreated 2.3 ± 2.2 % (72h); p=0.0086 and p=0.0229 respectively), that was absent in mice treated simultaneously with DXR and BLF501 (DXR + BLF501 3.3 ± 0.5 % and 2.2 ± 0.5 % at 48 and 72 h respectively; p=0.004 and p=0.028 *vs* DXR at 48h and 72h, respectively) (Figure 10). No modification of the proliferation of intestinal epithelial cells was observed in samples from mice treated with BLF501 alone.

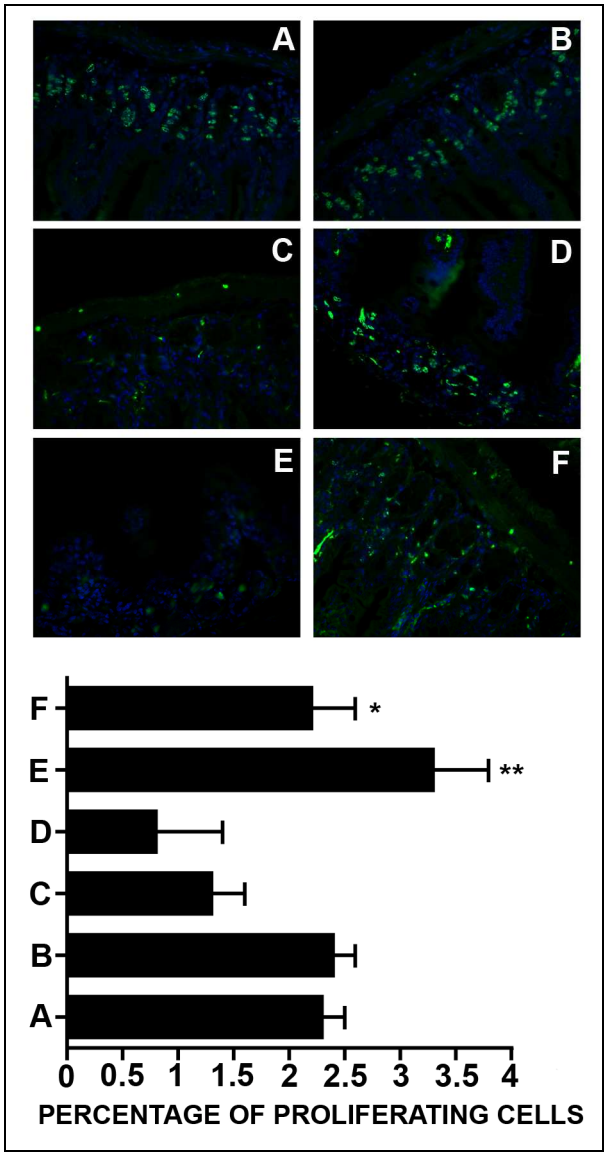

Figure 10: *BrdU immunofluorescence for evaluation of cellular proliferation (**A**) UNTR, untreated; (**B**) BLF501 25 µg/Kg (**C**) DXR 48h; (**D**) DXR + BLF501 25 µg/Kg 48h; (**E**) DXR 72h (**F**) DXR + BLF501 25 µg/Kg 72h. Statistical analysis: DXR+BLF501 25 µg/Kg 48h vs DXR 48h ** P=0.004; DXR+ BLF501 25 µg/Kg 72h vs DXR 72h * P=0.0282*

Treatment with BLF501 was also found to restore the expression of beta-catenin, a unique intracellular protein functioning as an integral component of the cell-cell adhesion complex and a principal signaling protein mediating canonical Wnt signaling linked with cellular proliferation. In fact, expression of beta-catenin was reduced at 48 hours after DXR administration in the villi and at 72 hours in both villi and crypts (Figure 11).

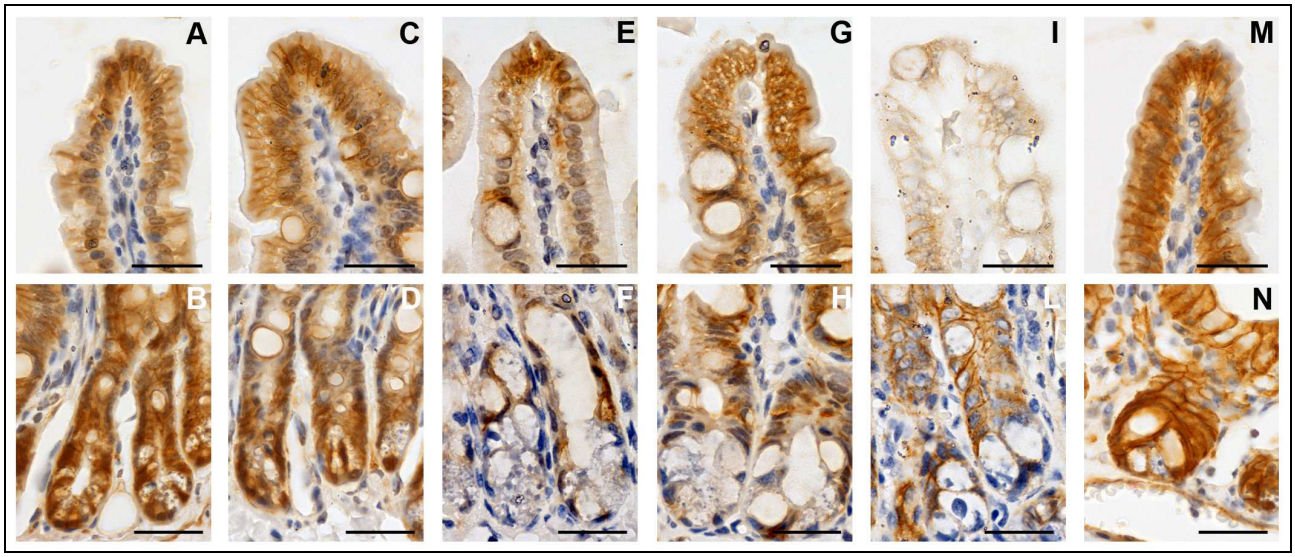

Figure 11: *Immunohistochemistry for the expression of beta-catenin in a model of acute mucositis. (**A-B**) UNTR, untreated; (**C-D**) BLF501 25 µg/Kg (**E-F**) DXR+5-FU 48h; (**G-H**) DXR+5-FU + BLF501 25 µg/Kg 48h; (**I-L**) DXR+5-FU 72h (**M-N**) DXR+5-FU +BLF501 25 µg/Kg 72h. Bars = 20 µm.*

The protective effect of BLF501 was then investigated by analyzing the expression of different genes implicated in the early response to tissue injury. In particular, we analyzed the expression of DLL-1, a marker for crypt cells that are in active proliferation like stem cells; TFF-3 and beta-actin, which are components of the mucus layer and cytoskeleton, respectively, and whose reduced expression mirrors decreased mucin production and alteration of cytoskeletal structure, respectively; sucrose isomaltase, a marker for brush border integrity and a key enzyme in carbohydrate metabolism, whose reduced expression mirrors epithelial damage and malabsorption of nutrients. Expression of all of these markers was reduced 48 hours after DXR treatment, but was similar to control mice in animals that had been co-administered BLF501 (Figure 12).

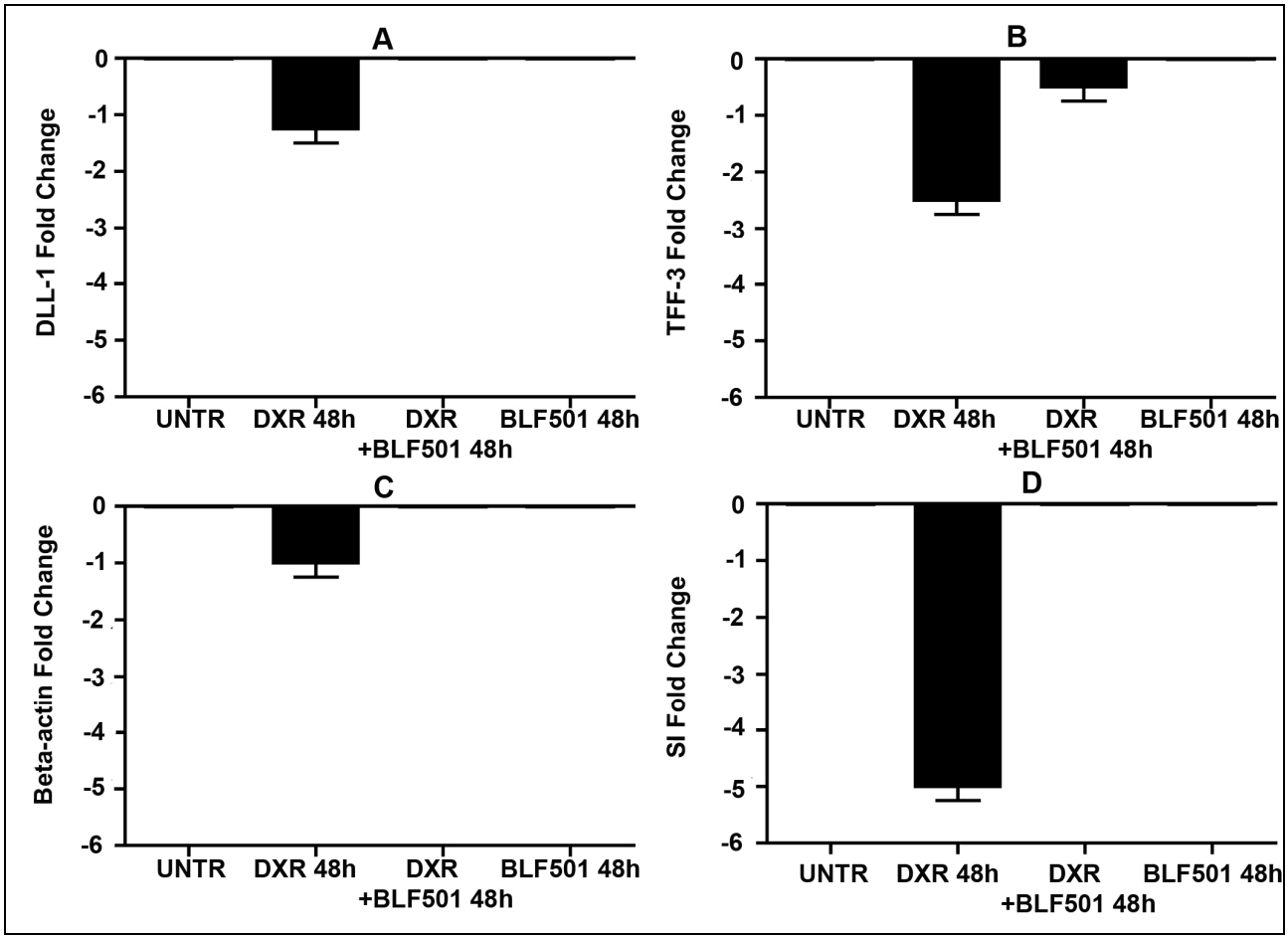

Figure 12: *Real-Time PCR analysis of changes in gene expression (**A**) DLL-1: (**B**) TFF-3; (**C**) Beta-actin; (**D**) Sucrase Isomerase;*

3.2 BLF501-induced recovery from injuries to the mucosa of the small intestine induced by repeated treatments with DXR and 5-FU.

In the following, we evaluated the effect of BLF501 in a model of DXR and 5-FU-induced mucositis that mimics medium-term, chemotherapy-induced effects on the intestinal mucosa. Intestinal epithelia from mice treated with the two chemotherapeutics were extensively damaged (Figure x). In particular, villi were atrophic, fused and reduced in height (-36.15 ± 2.56 % vs untreated); epithelial cells were hyperplastic and brush borders had large areas of erosion; focal ectasia of chyliferous vessels was detectable, numbers of goblet cells were decreased (DXR+5-FU 2.56 ± 1.28 %; untreated 7.13 ± 0.64 %), cells undergoing mitosis and cellular infiltrates rich in lymphocytes and plasma cells were also observed. Mice treated also with 25µg/Kg BLF501 showed substantial recovery from

chemotherapy-induced injury to the intestinal mucosa (villus eight: -12.31 ± 1.58 %; p = 0.0014 vs untreated; globet cells: 6.93 ± 0.63 %; p = 0.0383 vs untreated). At 2.5 µg/Kg, BLF501 improved morphological parameters (villus height: -16.82 ± 1.33 % , p = 0.0026 vs untreated), but was ineffective against loss of globet cells (2.2 ± 1.72 %) and appearance of mitotic cells; the 0.25 µg/Kg dosage of BLF501 was ineffective on all investigated parameters. Samples from the intestinal epithelia of mice treated with BLF501 alone were identical to those of control mice. A synopsis of these results is shown in Figure 13.

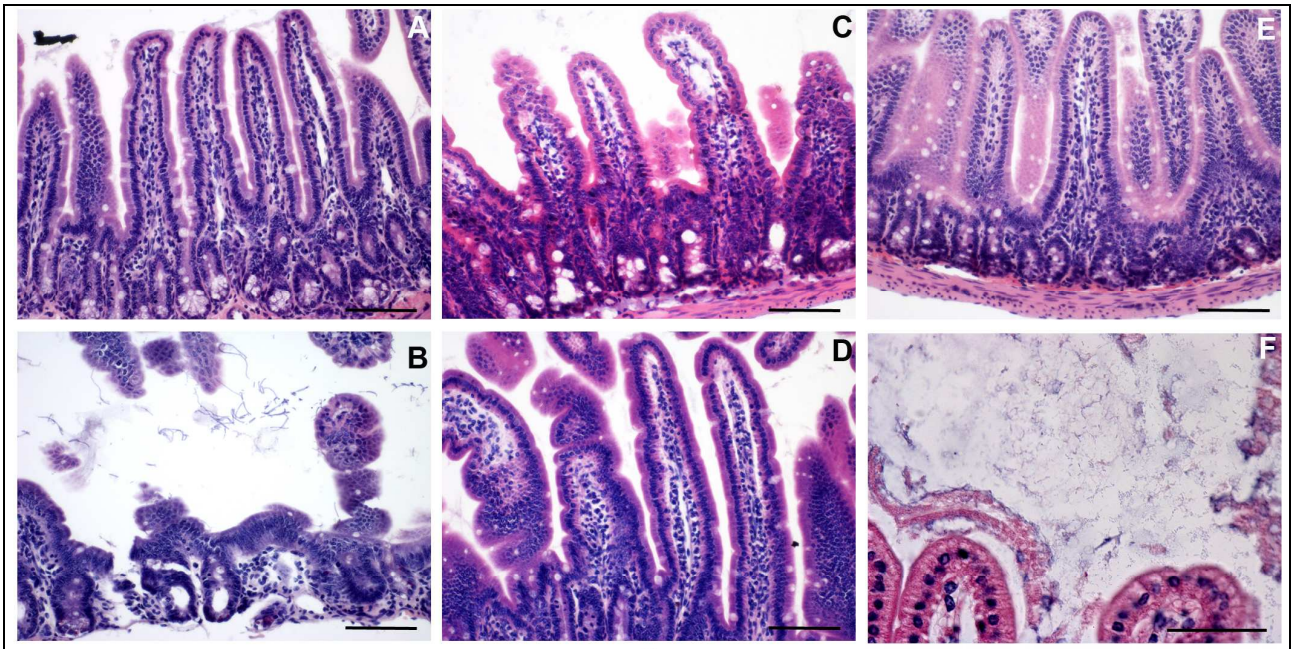

G

GROUP	Villus atrophy	Villus length reduction (% and SEM)	Loss of the brush border	Percentage of goblet cells (% and SEM)	Crypts morphology alteration	Presence of mitotic cells	Ectasia of the chyliferous vessels
UNTR	0	0	0	7.13 ± 0.64	0	0	0
DXR+5FU	+++	36.15 ± 2.56	+++	2.56 ± 1.28	++	+	+++
DXR+5FU +BLF501 25 µg/Kg	+	12.31 ± 1.58 **	+	6.93 ± 0.63 *	0	++	+
DXR+5FU +BLF501 2.5 µg/Kg	+	16.82 ± 1.33 **	+	2.2 ± 1.72	+	+	+
BLF501 25 µg/Kg	0	1.83 ± 1.86	0	8.09 ± 0.65	0	+	0/+

Figure 13: Hematoxilin/eosin staining of jejunum samples: (**A**) UNTR, untreated; (**B**) DXR+5-FU; (**C**) DXR+5-FU + BLF501 2.5 µg/Kg; (**D**) DXR+5-FU +BLF501 25 µg/Kg; (**E**) BLF501 25 µg/Kg; (**F**) DXR+5-FU luminal bacterial content. (**G**) Synoptic panel of evaluated parameters. Statistical analysis: villus length DXR+5-FU +BLF501 25 µg/Kg vs DXR+5FU ** p=0.0014. DXR+5FU +BLF501 2.5 µg/Kg vs DXR+5-FU ** p=0.0026. Percentage of goblet cells: DXR+5-FU +BLF501 25 µg/Kg vs DXR+5-FU * p=0.0383. Damage score legend: +++= SEVERE; ++= MILD; += LIGHT; 0= ABSENT. Bars = 20 µm.

We also analyzed the junctional systems of the intestinal epithelia of mice treated with the chemotherapeutics alone or with BLF501. In particular, we investigated the expression of ZO-1, which mirrors the integrity of tight junctions and beta-catenin, a component of adherens junctions. Immunofluorescent and Immunohistochemical staining of junctional systems revealed respectively that ZO-1 and beta-catenin were less expressed and had an altered distribution in intestinal samples from DXR/5-FU-treated mice. In contrast, samples from mice that were co-administered with BLF501 at 25 µg/Kg showed the typical honeycomb distribution of ZO-1 and expression/ distribution of beta-catenin similar to control mice. The 2.5 µg/Kg BLF501 dose was less effective. BLF501 (25 µg/Kg) alone did not alter the expression or distribution of either ZO-1 or beta-catenin (Figure 14)

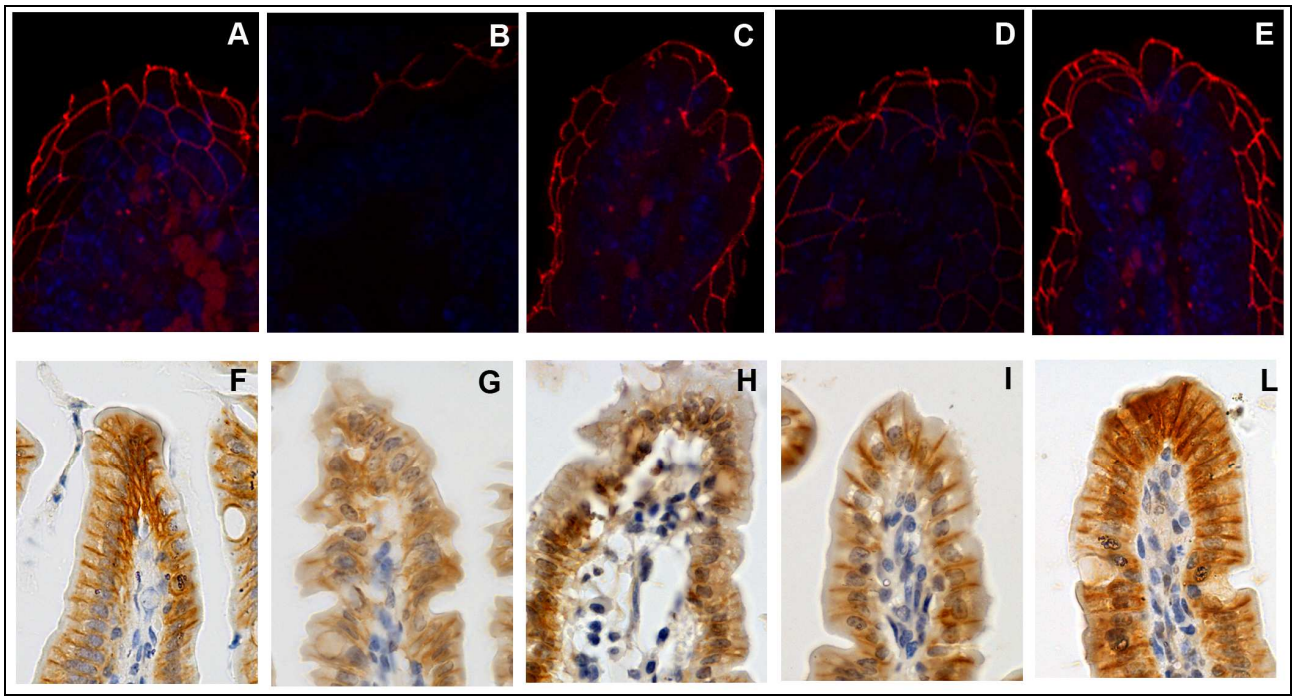

Figure 14: *ZO-1 immunofluorescence assay: (**A**) UNTR, untreated; (**B**) DXR+5-FU; (**C**) BLF501 25 µg/Kg; (**D**) DXR+5-FU +BLF501 2.5 µg/Kg; (**E**) DXR+5-FU + BLF501 25 µg/Kg. Magnification 60X Immunohistochemistry reaction for beta-catenin expression in a model of chronic mucositis. (**F**) UNTR, untreated; (**G**) DXR+5-FU; (**H**) DXR+5-FU + BLF501 2.5 µg/Kg; (**I**) DXR+5-FU +BLF501 25 µg/Kg; (**L**) BLF501 25 µg/Kg.*

3.3 BLF501 reduces the expression of specific markers for epithelial damages connected with chemotherapy-induced mucositis.

It's possible to appreciate that BLF 501 could restore the proper expression of a panel of proteins involved in cellular response after treatment with chemotherapic agents like doxorubicin and 5-fluorouracil. Akt is involved in cellular response events after a generic damage and, in the specific case, after treatment with 5-FU. Western Blots for Akt and P-Akt indicated that this protein is strongly expressed after treatments with doxorubicin and 5-fluorouracil. BLF501 treatment reduced Akt/ P-Akt levels in a dose-dependent manner. Caspase-3 is a marker for apoptosis and its expression is increased by chemotherapic treatment. BLF501 co-administration only at 25 µg/Kg dosage was effective to reduce Caspase 3 expression. Ezrin is a protein involved in tight junctions and adherent junctions remodelling and functional management; over-expression of Ezrin induces TJ and AJ opening and an alteration of intercellular permeability. Doxorubicin and 5-fluorouracil chronic administration induced Ezrin over-expression and BLF501 restored low levels of this protein in dose-dependent manner (Figure 15). BLF501 at 0.25 µg/Kg dose was completely ineffective (data not shown). Beta-actin assay was performed to assess uniformity of proteins concentration.

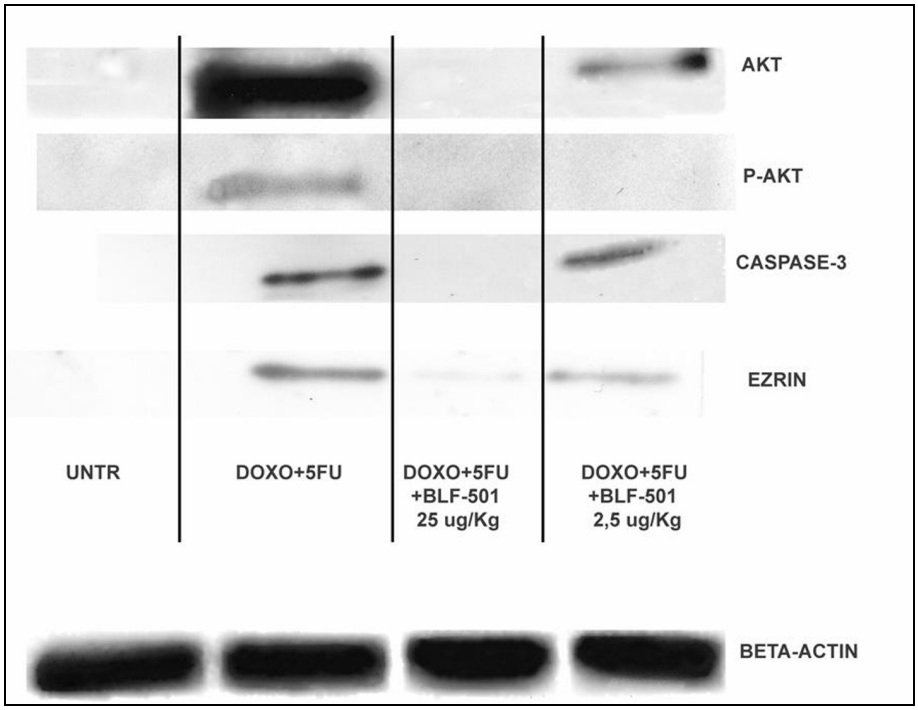

Figure 15*: western blot assay for epithelial damage markers.*

3.4 Oral administration of BLF501 does not interfere with the antineoplastic activity of DXR.

Overexpression of SGLT-1 is one survival strategy put in place by several tumoral cellular types, in particular EGFR-positive ones (31). To evaluate whether oral administration of BLF501 could interfere with the antitumor activity of the chemotherapeutics, we performed experiments in athymic mice that were injected subcutaneously with A431 cells, which strongly express both EGFR and SGLT-1 (32). Tumor growth rate in mice co-administered with DXR and BLF501 was similar to that in mice treated with DXR alone ($p=0.1836$). This shows that oral administration of BLF501 does not interfere with the antitumor activity of DXR (Figure 7). Interestingly, while DXR-treated mice showed an average reduction of 1g of body weight at the end of the experiment, a slight increase in the weight (~0.4 g) was observed in the group treated with DXR and BLF501. No differences in tumor growth rate were observed between untreated mice and mice treated with BLF501 alone.

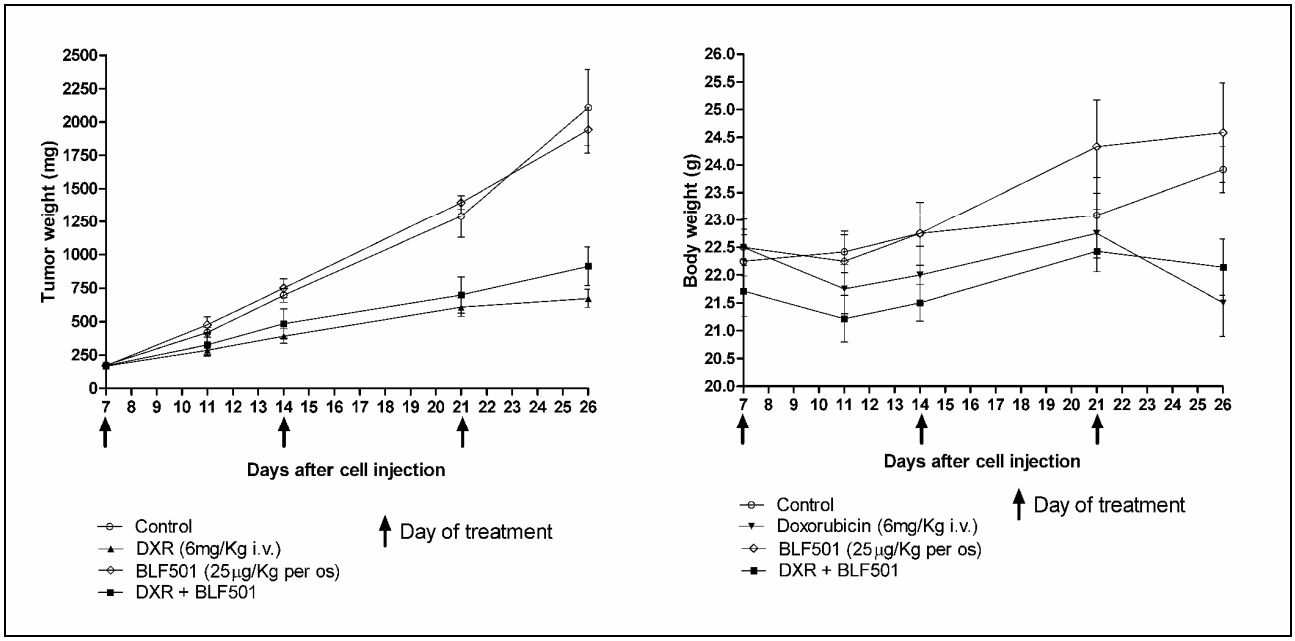

Figure 16. *Evaluation of tumor growth rate and body weight rate in simulated chemotherapy experiments.*

3.5 SGLT-1 activation in stably transfected Caco-2/bbe cells is fundamental for cytoprotection after doxorubicin plus BLF501 challenge.

BLF501 is a selective ligand for SGLT-1 (71) and *in vivo* experiments confirm the biological activity of the synthetic molecule. Despite this animal model is a complex system and BLF501 interaction with others targets could be not excluded. *In vitro* experiments were performed to assess SGLT-1 activation ability to maintain normal cells viability rates after DXR treatment and to further demonstrate the unique and selective functional interaction between SGLT-1 and BLF501. Caco-2/bbe cells stably transfected with SGLT-1 were treated with DXR with or without BLF501 co-administration for 48 hours.

Dose-response Neutral Red cell viability assays were performed in order to determine DXR cytotoxic dose and BLF501 effective concentration (data not shown). Selected doses for DXR and BLF501 were 100 µM and 11.5 µM respectively and they maintained used for all in vitro experiments. Not-transfected Caco-2/bbe cells were used as negative control, in order to confirm and clarify the pivotal role of SGLT-1 in protective action.

Neutral red viability assay was performed 48 hours after treatments; not-transfected Caco-2 cells resulted sensitive to DXR (viability rate reduced of 74% *vs* untreated cells) and BLF501 co-administration was ineffective to preserve cells viability (viability rate reduced of 75% *vs* untreated cells). Stably transfected Caco-2/bbe cells resulted sensitive to DXR treatment (viability rate reduced of 29% *vs* untreated cells) and BLF501 co-administration preserves cells viability.

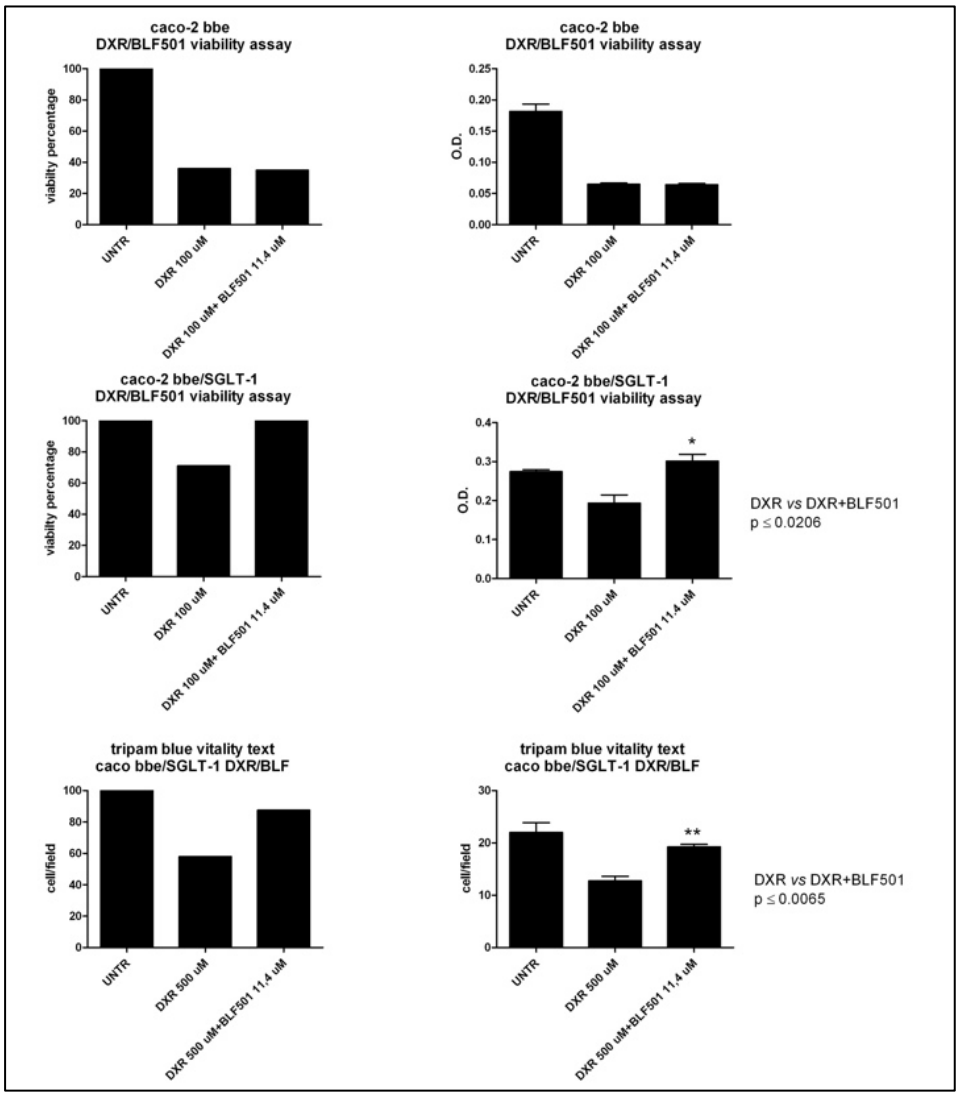

Figure 17. *Neutral Red viability assays on transfected and not-transfected Caco2 cells*

3.6 BLF501 protection against inflammatory bowel disease in vivo. **Oral administration of BLF-501 protects mice from DSS-induced diarrhoea.**

In vitro and vivo results in GIM model lead us to hypothesize that SGLT-1 may be an important target in intestinal diseases involving alteration of epithelial barrier effect. We tested BLF501's activity in a chemically induced mouse model of acute and chronic intestinal inflammation choosing a dextran sodium sulphate (DSS)-induced colitis model for its simplicity and reproducibility of the colonic lesions. DSS polymers are directly toxic to the gut epithelial cells, affecting firstly the integrity of the mucosal barrier and then stimulating local inflammation as a secondary phenomenon. For this reason we can improve BLF.501 activity in intestinal barrier protection, which is thought to be the initial inciting event in many intestinal disorders, including IBD.

A DSS concentration of 2% (w/v) addicted in the drinking water for 7 days induced strong colitis. To evaluate the effects of BLF-501 in this model, mice (10/group) were treated in the drinking water for 7 days with DSS 2% concomitantly or not with oral administration of BLF-501 (250 or 25 µg/kg) once a day in the last four days (as described in materials and methods). DSS intake did not differ in different groups of mice. Colitis in the DSS model is usually associated with wasting disease. Determination of weight every day to get a rough idea of colitis severity and is often indicative of differences in colitis development between experimental groups. Body weight significantly decreased in DSS group compared to control mice. The oral treatment with BLF-501 at doses of 250 µg/kg and 25 µg/kg recovers DSS-induced weight loss; the 2.5 µg/kg dose appeared to be ineffective.

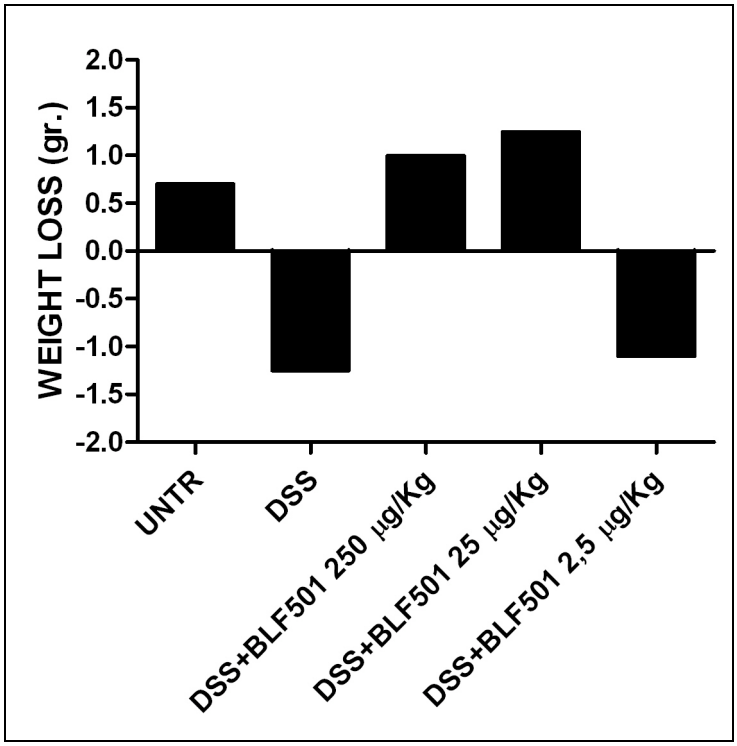

Figure 18. *Weight rate after DSS treatment with or without co- treatment with BLF501*

The DSS-induced damages are generally located in the distal colon, whose length decreases as the disease develops. Colon mean length of mice group treated only with DSS decrease of 32% compared to untreated ones. BLF-501 at 250 µg/kg and 25 µg/kg oral treatments of mice significantly reduced colonic shortening induced by DSS. Group of mice treated with BLF501 2.5 µg/kg and DSS showed colon length similar to DSS group.

About body weight and colon length results load us to consider 25 µg/kg the lower effective dose of our analogue glucose in this animal model.

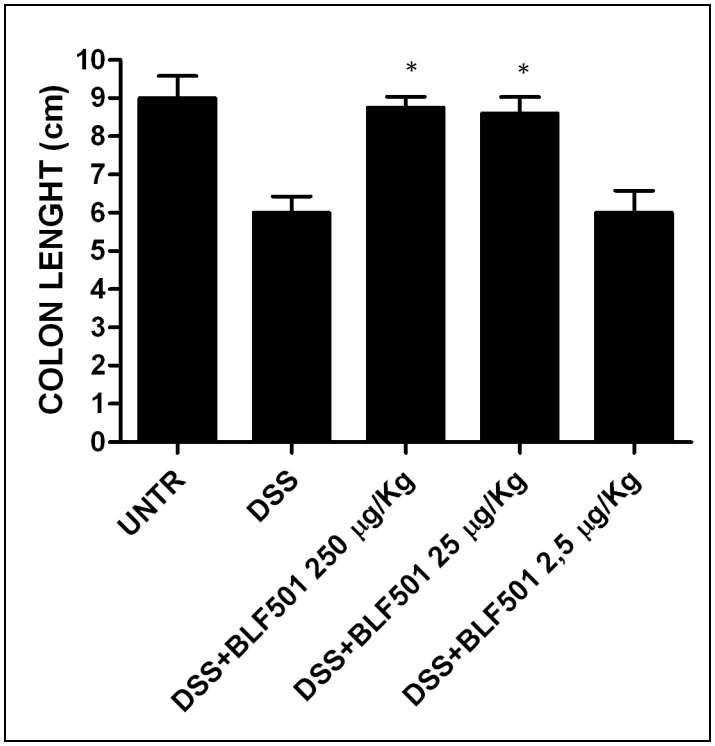

Figure 19. *Colon length evaluation after DSS treatment with or without co- treatment with BLF501*

After evaluation of colon length, colitis level of different group was scored using stool consistence as a standard parameter. DSS treated animals group have very soft stools with a 1,9 mean score, whereas untreated group shows normal stools with mean score 0 These results showed that oral treatment with BLF501 250 or 25 µg/kg inhibit water loss, maintaining normal stool consistence.

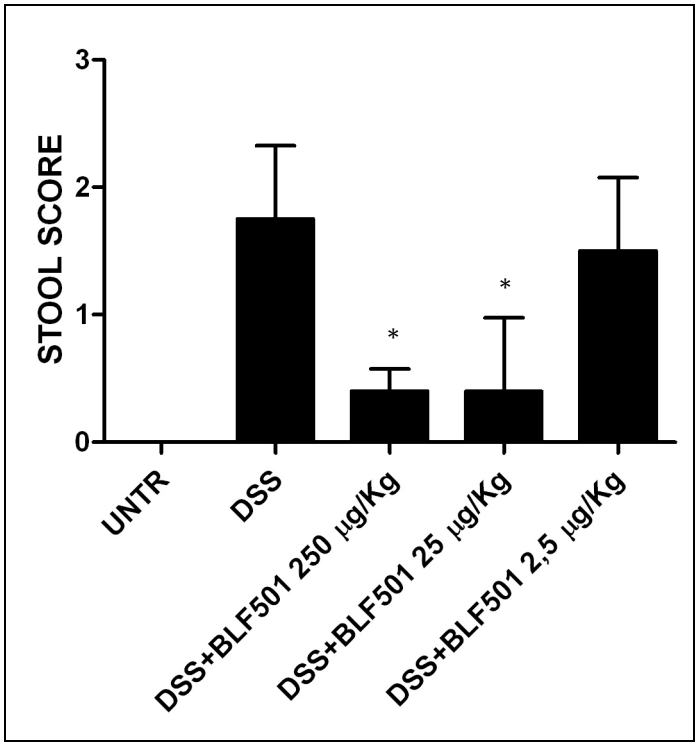

Figure 20. *Stool score after DSS treatment with or without co- treatment with BLF501*

The most important damage DSS-induced is characterized by changes in colon epithelium showing loss of crypts and reduction of globet cells, signs of surface epithelial regeneration, focal ulcerations, infiltration of inflammatory cells into the mucosa, and oedema in the sub-mucosa. Histopathological analysis using hematoxylin-eosin staining of colon section showed that DSS treatment induced crypt damage, ulceration, and infiltration of inflammatory cells in the distal colon. A histological colitis score was calculated for 10 slides for each mouse of different groups; score increasing has associated with inflammation develop (mean score of DSS group = 3.5 *vs* untreated = 0). Scoring system of colon section of DSS-treated group plus BLF-501 250 or 25 µg/kg shows protective role of SGLT-1 in this animal model of acute colitis.

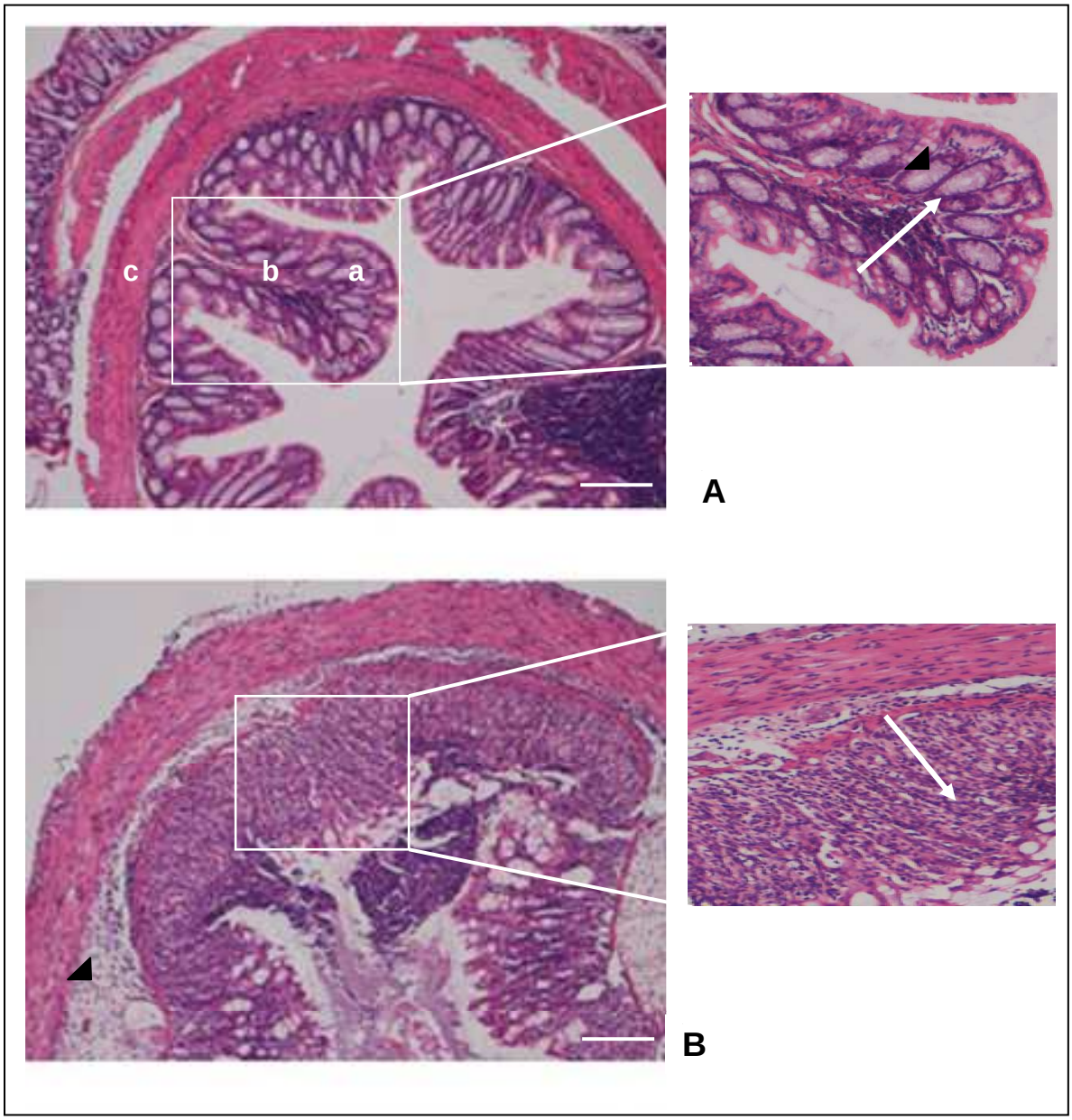
c
b
a
A
B

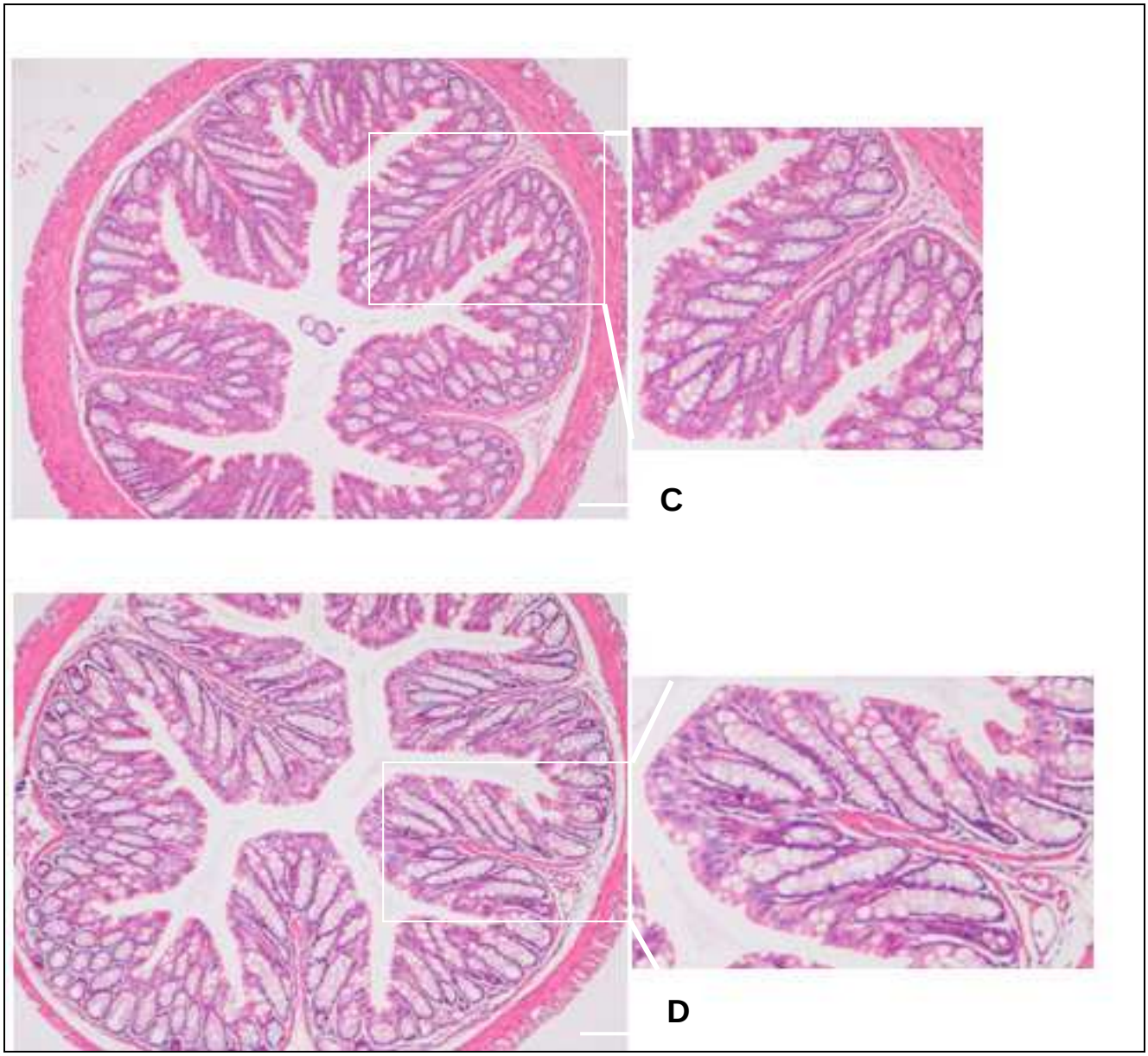

Figure 21. *(**A**) Rapresentative colonic H&E section from mice receiving water without DSS . **a**) Lamina mucosa; **b**)Lamina submucosa; **c**)Circular and longitudinal mussle. In magnification arrow shows colon crypte with normal morphology and black arrowhead indicates globet cells. (**B**) Colon histology from DSS-treated group. DSS induces thickening of the colon wall, globet cells and crypt loss in large areas (in magnification arrow). Infiltration reaching the lamina submucosa (withe arrow). (C) H&E of BLF501 250 µg/kg and (D) BLF501 25 µg/kg, histologically comparable with control group.*

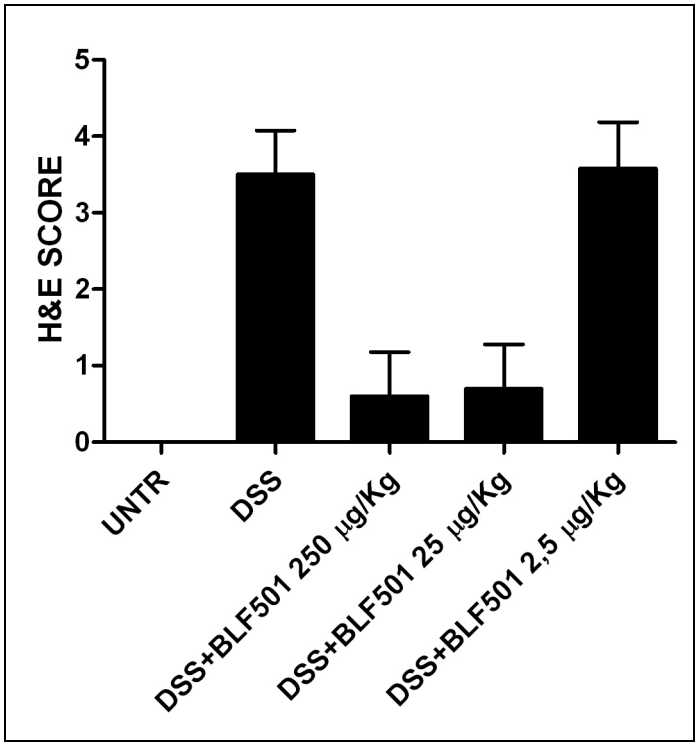

Figure 22. *Histological scores of the colon section stained with H&E. Results are representative of 10 section for each animal of different groups. DSS mean score shows high level of inflammation with transmurall leukocite infiltration and loss of globet cells. BLF501 250 and 25 µg/kg oral treatment prevents and protects from DSS-induced mucosal damage.*

DSS is directly toxic to gut epithelial cells of mucosal epithelium and induces a alteration of the mucosal barrier, with increase of antigens from colon lumen to lamina propria. In this animal model intestinal permeability alteration is the first step in colitis aetiology/onset. Previous data have already described that increased colon permeability is associated with colitis development after administration of DSS. Ussing Chamber analysis of the colon of DSS-treated mice presented very low transmembrane resistance (25 ± 2,24 Ωcm^2 vs 53.4 ±2,73 Ωcm^2 for untreated mice), indicating an increased permeability, whereas in mice group treated with DSS and oral administration of glucose and BLF501 250 and 25 µg/kg the transmembrane resistance remained similar to untreated mice (respectively 49,6 ± 1,52 Ω cm ^{2} or 50,4 ± 1,52 or 50,2 ± 1,2 vs 53.4 ±2,73 Ω cm^2 in untreated mice). This suggests that the increase of colon permeability DSS-induced is reverted by BLF501 oral administration.

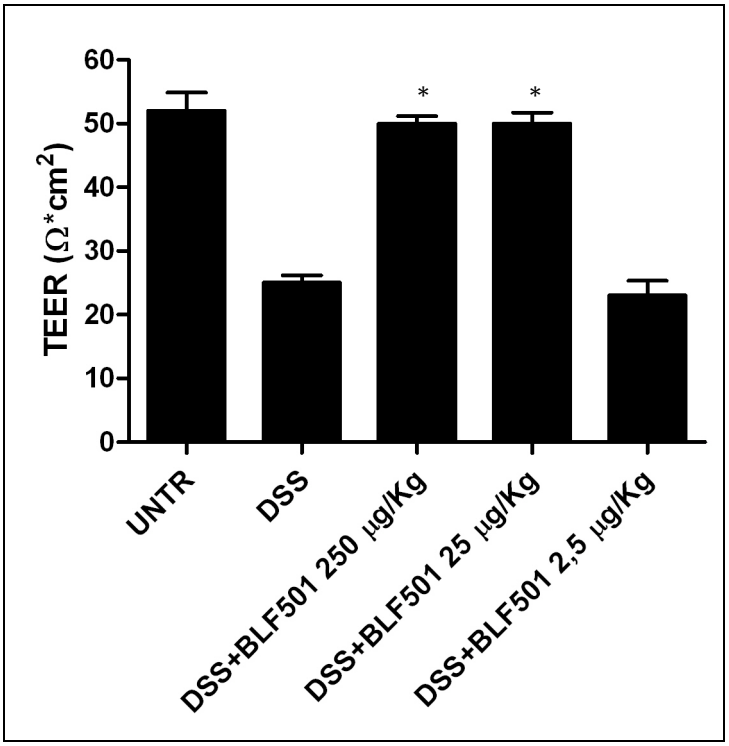

Figure 23. *Colon resistence. Values represent the mean of 5 animals/group. Data are the means (±SD). *, p < 0,01 vs DSS.*

3.7 BLF501 oral administration protects against chemically-induced mouse model of chronic intestinal inflammation.

SGLT-1.activation by BLF501 protects against DSS-induced acute colitis with important recovery of epithelial barrier intestinal barrier function. Several data in literature show that in different animal model of Crohn disease increased intestinal permeability has been shown before inflammation expression and the reversal of this defect can attenuate the disease, implying that the increased permeability is not simply epiphenomena but rather is a important etiological event. The administration of DSS at a concentration of 2% in the drinking water for three cycles is a validated chemically-induced mouse model of chronic intestinal inflammation. To evaluate the effect of BLF-501 in this model we valuated different parameters with attention for epithelial permeability function and morphology. After chronic colitis induction in DSS administered mice the colon length was significantly reduced if compared to samples from untreated mice. A significant decrease in the

shortening of the colon length was observed in mice that had received BLF501 almost for 3 week compared with DSS-administered mice (Figure 24).

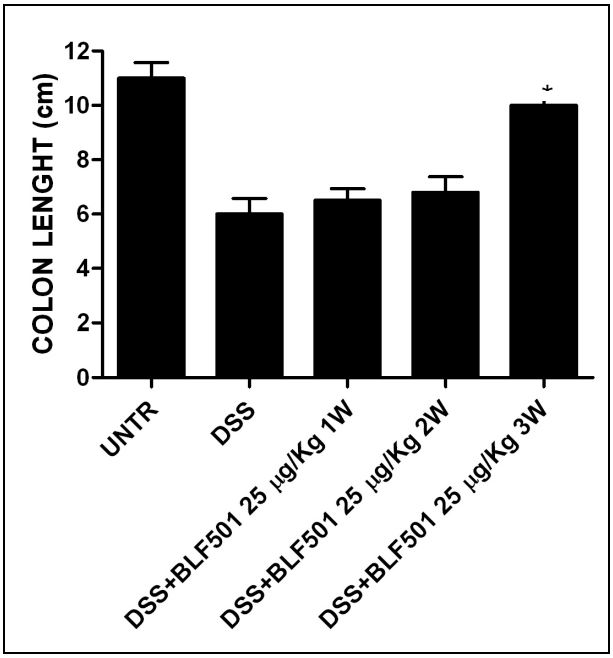

Figure 24. *Distal colon length.*
*Values represent the mean of 5 animals/group. Data are the means (±SD). *, p < 0,01 vs DSS*

From Histopathological analysis of hematoxylin/eosin-stained colon section is observable in DSS-treated mice samples the loss of crypts and reduction of globet cells, focal ulcerations, moderate infiltration of inflammatory cells to the mucosa, and oedema in submucosa. A significant decrease in histological score was observed in DSS plus BLF501 treated mice compared with those who received only DSS (Figure 25)

A

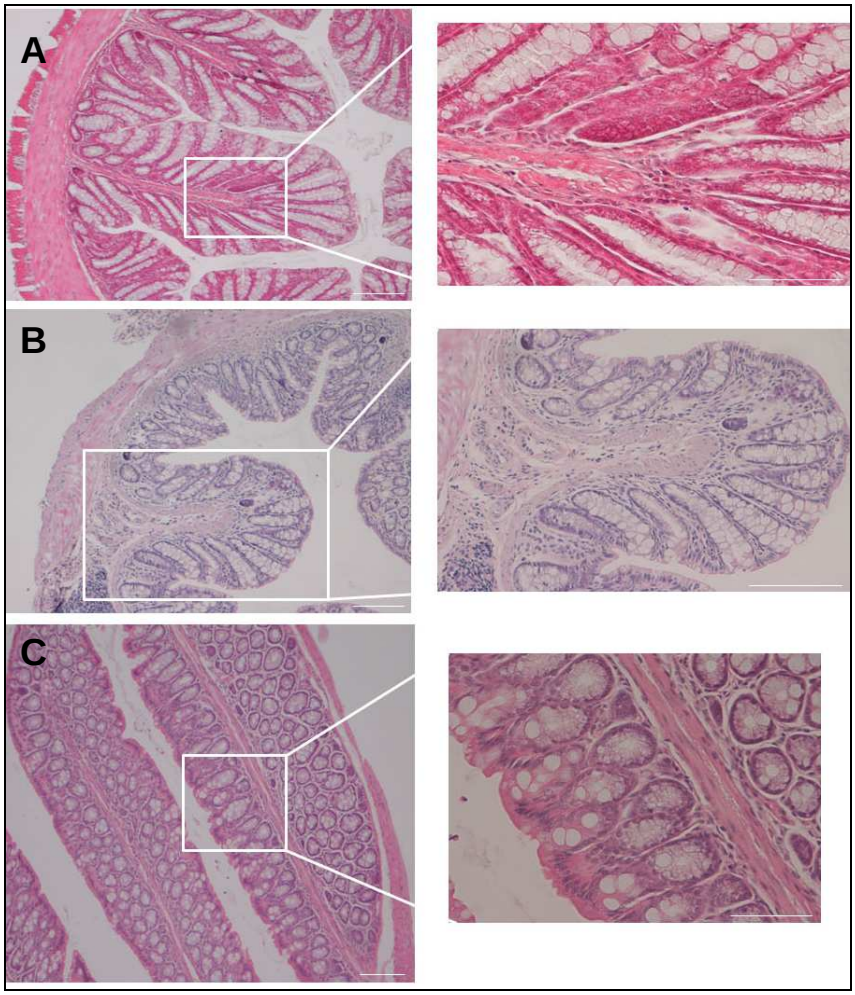

Figure 25. *Hystological analisis colon section stained H&E*
(A) UNTR; (B) DSS; (C) DSS+BLF501 25μg/Kg 3W

The intestinal epithelial barrier function is compromised in chronic inflammation, manifested by an increase in intestinal epithelial permeability. We analyzed the intestinal permeability by Ussing Chamber analysis, in order to determine if BLF501 is able to restore the intestinal barrier function. Segments of colon were mounted in Ussing chambers and electrophysiologic parameters were measured. As shown in figure 26 DSS treatment significantly reduced the barrier function of colon tissue, leading to an increase of TEER, while mice BLF501 presented a substantially normal mean value of resistance.

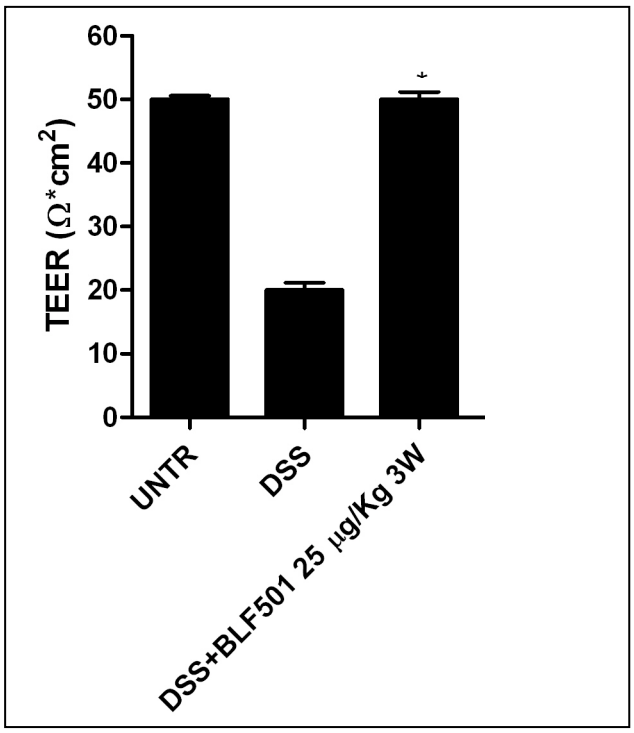

Figure 26. *Colon resistance values in chronic DSS model. Data are the means (±SD). *, p < 0,01 vs DSS*.

The decreased barrier function in colon of DSS-treated mice led us to determine if alteration in tight junction (TJ) structure accompanied this pathological alteration. Colon sections of different treatment were examined Immunohistochemically. In the colon of untreated mice, the transmembrane protein occludin and ZO-1 were precisely localized to the epithelial TJ. In well-oriented sections this is easily appreciated at low magnification as a regular series of bright red spots at the apical aspect of cell junctions. Examination at higher magnification revealed occludin and ZO-1 co-localization with the apical perijunctional actomyosin ring colonic epithelial of control. In contrast, DSS-treated mice show loss of crypts morphology and loss of bright red spots, occludin and ZO-1, at the apical aspect of cell junctions. Co-treatment with BLF501 after 3 weeks restores normal expression and distribution of the evaluated proteins.

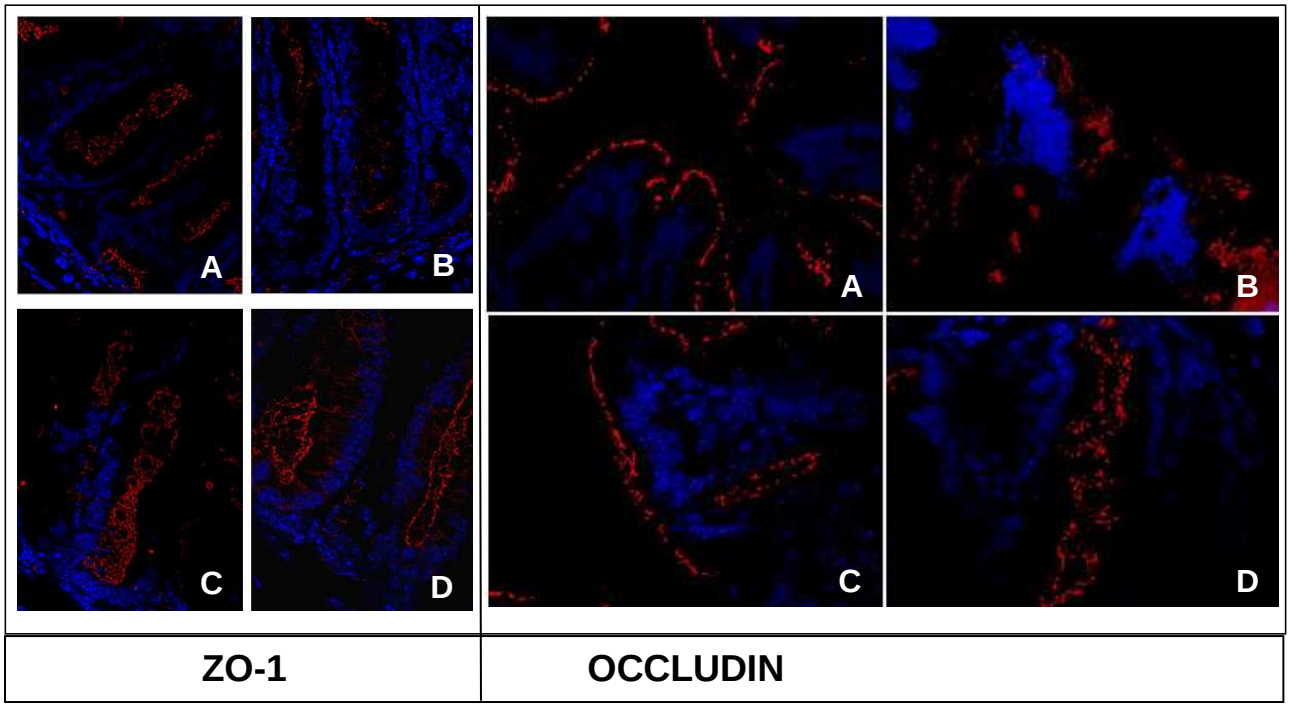

Figure 27. *Immunofluorescent staining for ZO-1 and Occludin Colon section of untreated mice, (**A**) UNTR; (**B**) DSS;(**C-D**) DSS+BLF501 25µg/Kg 3W*

4. DISCUSSION

The intestinal epithelial cells must integrate two different fundamental functions. They guarantee the absorption of nutrients transporting, often actively, a variety of substances from the intestinal lumen to the blood flow and, on the other hand, these cells form a physical barrier that results the first mechanism of protection that the innate immunity response executes against pathological agents that reach the mucosa through water and food ingestion.

The physical barrier represented by intestinal epithelium must not be considered as an unchanging entity, resistant to external stimuli. We highlight the ability of the intestinal epithelium of reacting to stimuli of different nature, physiological or harmful, and in particular we attribute to SGLT-1 a key role in the management of homeostasis of the intestinal barrier.

The classic role of SGLT-1 is to absorb D-glucose against a concentration gradient together with Na. The expression of SGLT-1 on the apical membrane of enterocytes, the cells that line the gut and overlook to the intestinal lumen, is fundamental in order to obtain the maximum D-glucose absorption from the digested alimentary bolo that transits through the gut.

Our researches and recent results published by other groups help us to shed new light on the “not-canonical role” of SGLT-1.

Recent papers outline the protective effect of active-type glucose transporter-1 (SGLT-1) engagement with high oral doses of D-glucose and non metabolizable 3-O-methyl-D-glucopyranose (3OMG) on damages induced by TLRs ligands in intestinal epithelial cells, in a murine model of septic shock and in LPS-induced liver injury, as well as liver injury and death induced by an overdose of acetaminophen (65; 66). This was found being due to glucose-induced down-regulation of systemic production of inflammatory cytokines, and

parallel enhanced production of anti-inflammatory cytokines. However, the high amounts of D-glucose and 3OMG necessary to induce anti-inflammatory effects represent a serious limitation for an hypothetical therapeutic application. To exploit SGLT-1 as a pharmacological target, we synthesized a library of glycomimetics based on a glucose and galactose scaffold structure. The aim was to identify agonists with much higher activity than glucose that does not undergo its metabolism.

From the screening of the library we identified a glucose derivative named BLF501, exerting anti-inflammatory activity at a molar concentration five orders of magnitude lower than glucose (71).

In parallel studies SGLT-1 has been described to be involved in anti-inflammatory and anti-apoptotic signalling, in the repair of plasma membrane integrity and tight junction (TJ) integrity injured by heat stress or cisplatin chemo-treatment (64).

The findings herein reported suggest the use of the synthetic D-glucose analogue BLF501 for the treatment of chemotherapy-induced mucositis. We showed that engagement of SGLT-1 by BLF501 accelerated recovery of intestinal epithelial structures from injuries induced by DXR and 5-FU. This effect is independent from glucose metabolism, since BLF501 is a C-glycoside, and as such does not to enter the metabolic pathways of D-glucose (71). The ability of SGLT-1 agonists that do not enter glucose metabolic pathways, to protect the intestinal mucosa upon oral administration had already been observed in a model of LPS-induced injury. Thus, oral administration of 3-OMG protected from LPS-induced injury similarly to D-glucose (65).

It is noteworthy that the dose of BLF501 necessary to protect from DXR-induced injury was much lower than doses of D-glucose or 3-OMG to protect from LPS-induced injury (25 μg/Kg vs. 2.5 g/Kg). This capacity of BLF501 to act at very low doses is presumably due to its high affinity for SGLT-1. Although we have no direct data on the binding of BLF501 to SGLT-1, this possibility is supported by our previous finding that, *in vitro,* both D-glucose

and BLF501 blocked LPS-induced release of IL-8, but BLF-501 was active at a dose about 10^5-10^6-fold lower than D-glucose (71).

Regarding the mechanism underlying its therapeutic effect, orally administered BLF501 did not directly protect the intestinal epithelium from chemotherapy-induced injury but, rather, anticipated and facilitated the recovery, which was detectable at 48 hours and almost complete at 72 hours after a single administration of DXR.

Regarding the different modifications that were observed upon co-administration of BLF501 with chemotherapeutics, we found the reduced expression of caspase-3 in the intestines of these mice compared to those that were administered only chemotherapeutics. This is likely to reflect a reduction of apoptotic events and is in accordance with recent findings that glucose administration reduces LPS-induced apoptotic events in enterocytes both *in vitro and in vivo.* (72, 64).

We observed also restoration of the integrity of tight junctions in intestinal epithelia upon administration of BLF501 to mice that were treated also with DXR, or DXR and 5-FU. Overall, these results are consistent with those obtained by others showing that in the presence of heat- or chemical-induced sub-lethal stress conditions, activation of SGLT-1 restores the integrity of tight junctions. This has been shown in vitro experiments in which the integrity of tight junctions had been disrupted by cisplatin or heat shock proteins (64; 45). In particular, samples of the small intestine from mice treated with DXR and 5-FU showed altered expression and distribution of the junctional proteins ZO-1 and beta-catenin. On the other hand, in mice that had been administered also BLF501, ZO-1 and beta-catenin were normally expressed and distributed. Moreover, Ezrin, that has a physiological role in the remodelling of junctional mechanisms (30; 73-77), and was over-expressed upon treatment of DXR and 5-FU treatment causing the opening of junctional systems, returned to normal levels in mice that had been administered also BLF501.

On the other hand we did not observe any effect of orally administered BLF501 on the antitumor activity of the chemotherapeutics. No difference was observed between DXR- and DXR plus BLF501-treated mice whereas, as expected, tumours in untreated mice grew significantly faster that tumours in mice that had been administered DXR.

We believe that our findings are very relevant in view of a potential therapeutic use of BLF501 in the setting of chemo- or radiotherapy-induced mucositis. In fact, chemotherapeutics induce apoptotic cell death and inhibit proliferation in rapidly dividing epithelia like those in the intestine (78). The consequence is mucosal atrophy and the reduction of the absorptive capacity of the intestine. This leads to a further deterioration of the general conditions of patients that are already heavily compromised.

In our mucositis models, BLF501 has been found to restore proliferation and integrity of junctional systems, as well as reduce the expression of a marker of apoptosis. These positive consequences on the overall integrity of the epithelium were confirmed by our histological analyses. These findings suggest the use of BLF501 as a unique therapeutic device for the maintenance of the integrity of the intestinal epithelium in case of chemotherapy-induced injury. There are currently different therapeutic approaches for patients suffering from mucositis, but all of them have serious side effects and/or act only on to reduce symptoms. These approaches include opioids with their potent anti-nociceptive activity, the use of Lactobacillus, KGF, hyperbaric chamber, glutamine, and 5-acetyl salicylic acid (79-81)

The role of *in vivo* SGLT-1 activation by BLF501 is fundamental for the observed goals in GIM treatment. However, the complexity of *in vivo* models makes difficult to demonstrate clearly the interaction between SGLT-1 and BLF501. To establish a more direct link between receptor and substrate appropriate *in vitro* assays were performed. In WT Caco-2/bbe cells DXR treatment has a dramatic effect on cell viability and administration of BLF501 in absence of SGLT-1 transfection was totally ineffective and no protection was

observed. Transfection with SGLT-1 changed radically the situation described above. First of all surviving rate of cells treated with only DXR was higher in confront with not-transfected Caco-2 cells in presence of DXR, even though significantly reduced if compared with untreated cells. This result lead us to attribute to SGLT-1 an intrinsic protective role exerted by simple expression of this protein; furthermore SGLT-1 activation via BLF501 simultaneous administration enhanced cytoprotection maintaining a control-like growth rate. Results of this panel of *in vitro* experiments lead us to attribute a key role to SGLT-1 expression and activation, confirming the specificity of the ligand and the essential role of the interaction between BLF501 and SGLT-1.

In conclusion, our results show that oral administration of the non-metabolizable glucose analogue BLF501 leads to accelerated recovery of the intestinal mucosa from injuries induced by chemotherapeutic drugs. This suggests a possible prophylactic and/or therapeutic use of BLF501 for the prevention or reduction of severity of chemotherapy-induced mucositis.

In parallel with the good results obtained in the protection of the structural integrity of the intestine in GIM model with SGLT-1 activation, we performed similar experiments in a model of IBD based on DSS treatment.

Crohn’s disease is a chronic inflammatory process that affects the small intestine and colon and is associated with a "leaky gut", characterized by an increase in intestinal epithelial permeability. Actual pharmacological therapies vary in their ability to induce and maintain a sufficient control of symptoms balancing their activity with an intrinsic inevitable toxicity. Our data obtained from the present study suggest that the activation of SGLT-1 with BLF501 may constitute a new approach for an effective treatment of IBD.

DSS-colitis models share many clinical and pathological features of human ulcerative colitis with regard to ulceration and loss of barrier function. Feeding mice for several days with DSS polymers in the drinking water induces an acute colitis characterized by bloody

diarrhea, intestinal ulcerations and infiltrations with granulocytes. It is generally believed that DSS is directly toxic to gut epithelial cells of the basal crypts and affects the integrity of the mucosal barrier. The administration of DSS at a concentration of 2% in the drinking water for three cycles will result in development of chronic colitis. DSS, with is surfactant action on epithelial monolayer, has been shown to increase mucosal permeability in mice (82) and reduce TEER intestinal epithelium (83). For these reasons DSS-colitis model has been widely used to study mucosal healing (84). The DSS-colitis model is effective in mimic pathological features of human IBDs; although the exact action of DSS is not fully understood, it is believed that DSS causes mucosal injury and disrupts the barrier function, leading to inflammation. In the human condition it is evident that increased intestinal permeability is commonly observed in population at high risk of developing Crohn's disease. Increased permeability is observed in the absence of symptoms of disease, suggesting that it is not merely an early manifestation of Crohn's disease (Alteration in intestinal permeability).

In our previous work our data obtained by Ussing Chamber analysis of colon samples have shown that the increase in colon permeability, which may be observed in an enterocolitis mouse model, is avoided when animal are concomitantly treated with oral glucose. This result leads us to hypothesize that SGLT-1 activation exerted by BLF501 may protect intestinal mucosal barrier in mouse model of chronic and acute inflammatory diseases and DSS-based murine model is appropriate to investigate the effect of oral administration of BLF501.

Using this model, we found that mice with chronic colitis BLF501-treated not presents typical mucosal injury, shows a weight recovery and not develops severe clinical symptoms, including bleeding and dehydratation. Histopathological analysis of hematoxylin & eosin stained samples from diverse groups of animals confirmed these findings from an anatomophatological point of view. DSS-treated mice, both in chronic and

acute models present an altered macroscopical appearance of the colon epithelium; in particular an abnormal organization of the IECs monolayer is reported. Co-treatment with BLF501 restores an untreated-like condition in a dose dependent manner in mice treated in acute model; evidence confirmed in the chronic one at BLF501 the single dosage.

In GIM model the macroscopic alteration of the epithelial structure was probably the most impressive result of the treatment with chemotherapic agents. In DSS models the most important evaluated aspect is the permeability alteration. We investigated the capacity of BLF501 oral administration to control barrier intestinal permeability *in vivo* and data obtained by Ussing chamber analysis shown that acute and chronic treatment with DSS leads to increased colon permeability compared with control mice, oral administration of BLF501 induce in an intestinal permeability recovery in a dose-dependent manner.

TEER evaluation is an important direct parameter to test intestinal permeability but an analysis of specific proteic markers linked with junctional systems expression and distribution. Tight junctions seal the paracellular space and regulate the permeability of the mucosal barrier and are the highly ordered structure formed by multiprotein complexes consisting of transmembrane proteins, as occludin and nonmembrane proteins, as ZO-1. The TJ protein has been reported to be deregulated in IBD; this is the fundamental background event underlying TEER reduction. We evaluated occludin and ZO-1 only in chronic model because their altered expression is more evident that in acute model. Selected junctional proteins expression and distribution in colon tissue samples of different treatments was evaluated with specific immunostainings assays and we evaluated that DSS treatment alters both expression and localization of occludin and ZO-1. BLF501 exerts its protective action restoring normal quantitative expression and distribution of both proteins linking intestinal permeability recovery observed with Ussing Chamber analysis with TJ protection.

These results suggest that the BLF501-mediated action involves stabilization of epithelial junction complex. SGLT-1 activation plays an important role in restoring mucosal integrity after DSS treatment and this reparative mechanism could reestablish intact barrier function and structure.

5 CONCLUSIONS

In this work it was decided to evaluate the role of activation of SGLT-1 as a key factor in protecting the intestinal epithelium in the presence of potential sources of damage and the choice of two very different types of damage and numerous techniques for the assessment of the effects was dictated by the desire to have the broadest possible look at the potential of SGLT-1 activation by the synthetic molecule BLF501.

All the collected data describe different aspects linked with SGLT-1 activation:

1. SGLT-1 presence is fundamental for the protective action exerted by BLF501
2. SGLT-1 is activated by a very low amount of a synthetic molecule: an important aspect for pharmacologic and pharmacotherapeutic studies of ligands and receptor.
3. SGLT-1 activation has a direct effect on expression and distribution of member proteins of adherents and tight junctions, contributing to the correct formation and action of junctional systems.
4. SGLT-1 activation maintains the correct proliferation rate of intestinal epithelial cells.
5. SGLT-1 activation restores epithelial homeostasis balancing pro-apoptotic and anti-apoptotic pathways in presence of damage.

From these studies we can affirm that SGLT-1 has a key role in the management of events related to the structural integrity of the intestinal epithelium with particular attention to the aspects of maintaining the correct macroscopic structure, barrier function and tissue self-renewal ability after damages of different nature. SGLT-1 may constitute a target for new therapeutic approaches both for GIM and IBDs and, at the same time BLF501 could become a lead compound for SGLT-1-active ligands interaction studies.

6 REFERENCES

1. Pinto D, Clevers H. Wnt control of stem cells and differentiation in the intestinal epithelium. Exp Cell Res. 2005 Jun 10;306(2):357-63.
2. Pilewski, J. M. & Frizzell, R. A. Role of CFTR in airway disease. Physiol. Rev. 79, S215–S255 (1999).
3. Heazlewood, C. K. et al. Aberrant mucin assembly in mice causes endoplasmic reticulum stress and spontaneous inflammation resembling ulcerative colitis. PLoS Med. 5, e54 (2008).
4. Ayabe T, Satchell DP, Wilson CL, Parks WC, Selsted ME, Ouellette AJ.Secretion of microbicidal alpha-defensins by intestinal Paneth cells in response to bacteria. Nat Immunol. 2000 Aug;1(2):113-8.
5. Gewirtz AT, Rao AS, Simon PO Jr, Merlin D, Carnes D, Madara JL, Neish AS. Salmonella typhimurium induces epithelial IL-8 expression via Ca(2+)-mediated activation of the NF-kappaB pathway. J Clin Invest. 2000 Jan;105(1):79-92.
6. Hooper LV, Stappenbeck TS, Hong CV, Gordon JI. Angiogenins: a new class of microbicidal proteins involved in innate immunity. Nat Immunol. 2003 Mar;4(3):269-73
7. Barton GM, Medzhitov R. Control of adaptive immune responses by Toll-like receptors. Curr Opin Immunol. 2002 Jun;14(3):380-3
8. Matzinger P. The danger model: a renewed sense of self. Science. 2002 Apr 12;296(5566):301-5
9. Dockray GJ. Luminal sensing in the gut: an overview. J Physiol Pharmacol. 2003 Dec;54 Suppl 4:9-17
10. Suzuki T. Regulation of intestinal epithelial permeability by tight junctions. Cell Mol Life Sci. 2012 Jul 11
11. Assimakopoulos SF, Papageorgiou I, Charonis A. Enterocytes' tight junctions: From

molecules to diseases. World J Gastrointest Pathophysiol. 2011 Dec 15;2(6):123-37

12. Schneeberger EE, Lynch RD. The tight junction: a multifunctional complex. Am J Physiol Cell Physiol. 2004 Jun;286(6):C1213-28
13. Shin K, Fogg VC, Margolis B. Tight junctions and cell polarity. Annu Rev Cell Dev Biol. 2006;22:207-35
14. Keiper T, Santoso S, Nawroth PP, Orlova V, Chavakis T. The role of junctional adhesion molecules in cell-cell interactions. Histol Histopathol. 2005 Jan;20(1):197-203
15. Amasheh S, Fromm M, Günzel D. Claudins of intestine and nephron - a correlation of molecular tight junction structure and barrier function. Acta Physiol (Oxf). 2011 Jan;201(1):133-40
16. Markov AG, Veshnyakova A, Fromm M, Amasheh M, Amasheh S. Segmental expression of claudin proteins correlates with tight junction barrier properties in rat intestine. J Comp Physiol B. 2010 Apr;180(4):591-8
17. Angelow S, Yu AS. Structure-function studies of claudin extracellular domains by cysteine-scanning mutagenesis. J Biol Chem. 2009 Oct 16;284(42):29205-17
18. Veshnyakova A, Krug SM, Mueller SL, Piontek J, Protze J, Fromm M, Krause G. Determinants contributing to claudin ion channel formation. Ann N Y Acad Sci. 2012 Jun;1257:45-53
19. Will C, Fromm M, Müller D. Claudin tight junction proteins: novel aspects in paracellular transport. Perit Dial Int. 2008 Nov-Dec;28(6):577-84
20. González-Mariscal L, Quirós M, Díaz-Coránguez M. ZO proteins and redox-dependent processes. Antioxid Redox Signal. 2011 Sep 1;15(5):1235-53
21. Van Itallie CM, Colegio OR, Anderson JM. The cytoplasmic tails of claudins can influence tight junction barrier properties through effects on protein stability. J Membr Biol. 2004 May 1;199(1):29-38

22. Wu J, Yang Y, Zhang J, Ji P, Du W, Jiang P, Xie D, Huang H, Wu M, Zhang G, Wu J, Shi Y. Domain-swapped dimerization of the second PDZ domain of ZO2 may provide a structural basis for the polymerization of claudins. J Biol Chem. 2007 Dec 7;282(49):35988-99
23. Sabath E, Negoro H, Beaudry S, Paniagua M, Angelow S, Shah J, Grammatikakis N, Yu AS, Denker BM. Galpha12 regulates protein interactions within the MDCK cell tight junction and inhibits tight-junction assembly. J Cell Sci. 2008 Mar 15;121(Pt 6):814-24
24. Citi S, Pulimeno P, Paschoud S. Cingulin, paracingulin, and PLEKHA7: signaling and cytoskeletal adaptors at the apical junctional complex. Ann N Y Acad Sci. 2012 Jun;1257:125-32
25. Ivanov AI. Actin motors that drive formation and disassembly of epithelial apical junctions. Front Biosci. 2008 May 1;13:6662-81
26. Turner JR. Show me the pathway! Regulation of paracellular permeability by Na(+)-glucose cotransport. Adv Drug Deliv Rev. 2000 Jun 30;41(3):265-81
27. Uhing MR. Effect of sodium ion coupled nutrient transport on intestinal permeability in chronically catheterised rats. Gut. 1998 Jul;43(1):22-8
28. Kovbasnjuk ON, Szmulowicz U, Spring KR. Regulation of the MDCK cell tight junction. J Membr Biol. 1998 Jan 1;161(1):93-104
29. Turner JR, Black ED, Ward J, Tse CM, Uchwat FA, Alli HA, Donowitz M, Madara JL, Angle JM. Transepithelial resistance can be regulated by the intestinal brush-border Na(+)/H(+) exchanger NHE3. Am J Physiol Cell Physiol. 2000 Dec;279(6):C1918-24
30. Turner JR, Rill BK, Carlson SL, Carnes D, Kerner R, Mrsny RJ, Madara JL. Physiological regulation of epithelial tight junctions is associated with myosin light-chain phosphorylation. Am J Physiol. 1997 Oct;273(4 Pt 1):C1378-85

31. Clayburgh DR, Rosen S, Witkowski ED, Wang F, Blair S, Dudek S, Garcia JG, Alverdy JC, Turner JR. A differentiation-dependent splice variant of myosin light chain kinase, MLCK1, regulates epithelial tight junction permeability. J Biol Chem. 2004 Dec 31;279(53):55506-13
32. Berglund JJ, Riegler M, Zolotarevsky Y, Wenzl E, Turner JR. Regulation of human jejunal transmucosal resistance and MLC phosphorylation by Na(+)-glucose cotransport. Am J Physiol Gastrointest Liver Physiol. 2001 Dec;281(6):G1487-93
33. Li Q, Zhang Q, Wang M, Zhao S, Ma J, Luo N, Li N, Li Y, Xu G, Li J. Interferon-gamma and tumor necrosis factor-alpha disrupt epithelial barrier function by altering lipid composition in membrane microdomains of tight junction. Clin Immunol. 2008 Jan;126(1):67-80. Epub 2007 Oct 26.
34. Kobayashi K, Umezawa K, Yasui M. Apoptosis in mouse amniotic epithelium is induced by activated macrophages through the TNF receptor type 1/TNF pathway. Biol Reprod. 2011 Feb;84(2):248-54
35. Watson AJ, Hughes KR. TNF-α-induced intestinal epithelial cell shedding: implications for intestinal barrier function. Ann N Y Acad Sci. 2012 Jul;1258:1-8
36. Wang F, Graham WV, Wang Y, Witkowski ED, Schwarz BT, Turner JR. Interferon-gamma and tumor necrosis factor-alpha synergize to induce intestinal epithelial barrier dysfunction by up-regulating myosin light chain kinase expression. Am J Pathol. 2005 Feb;166(2):409-19
37. Scardina GA, Pisano T, Messina P. Oral mucositis. Review of literature. NY State Dent J. 2010 Jan;76(1):34-8. Review.
38. Sonis ST. Regimen-related gastrointestinal toxicities in cancer patients. Curr Opin Support Palliat Care. 2010 Mar;4(1):26-30. Review.
39. Sonis ST. Pathobiology of mucositis. Semin. Oncol. Nurs. 2004; 20:11–5
40. Carvalho C, Santos RX, Cardoso S, Correia S, Oliveira PJ, Santos MS, Moreira PI.

Doxorubicin: the good, the bad and the ugly effect. Curr Med Chem. 2009;16(25):3267-85. Epub 2009 Sep 1. Review.

41. Honda M, Miura A, Izumi Y, Kato T, Ryotokuji T, Monma K, Fujiwara J, Egashira H, Nemoto T. Doxorubicin, cisplatin, and fluorouracil combination therapy for metastatic esophageal squamous cell carcinoma. Dis Esophagus. 2010 Jun 10.
42. Jones JA, Avritscher EB, Cooksley CD, Michelet M, Bekele BN, Elting LS. Epidemiology Peterson DE, Bensadoun RJ, Roila F. Management of oral and gastrointestinal mucositis: ESMO clinical recommendations. ESMO Guidelines Working Group. Ann Oncol. 2009 May;20 Suppl 4:174-7. Review.
43. Melichar B, Dvorák J, Hyspler R, Zadák Z. Intestinal permeability in the assessment of intestinal toxicity of cytotoxic agents. Chemotherapy. 2005 Oct;51(6):336-8. Epub 2005 Oct 13.
44. Blijlevens NM, van't Land B, Donnelly JP, M'Rabet L, de Pauw BE. Measuring mucosal damage induced by cytotoxic therapy. Support Care Cancer. 2004 Apr;12(4):227-33. Epub 2004 Jan 30.
45. Ikari A, Nakano M, Suketa Y, Harada H, Takagi K. Reorganization of ZO-1 by sodium-dependent glucose transporter activation after heat stress in LLC-PK1 cells. J Cell Physiol. 2005 Jun;203(3):471-8.
46. Dekaney C. et al. Regeneration of intestinal stem/progenitor cells following doxorubicin treatment of mice. Am J Physiol Gastrointest Liver Physiol 297: G461–G470, 2009
47. Van Vliet MJ, Harmsen HJ, de Bont ES, Tissing WJ. The role of intestinal microbiota in the development and severity of chemotherapy-induced mucositis. PLoS Pathog. 2010 May 27;6(5):e1000879.
48. Jones JA, Avritscher EB, Cooksley CD, Michelet M, Bekele BN, Elting LS. Epidemiology of treatment-associated mucosal injury after treatment with newer

regimens for lymphoma, breast, lung, or colorectal cancer. Support Care Cancer. 2006 Jun;14(6):505-15. Epub 2006 Apr 7.

49. Podolsky DK. Inflammatory bowel disease. N Engl J Med. 2002 Aug 8;347(6):417-29.

50. Fuss IJ, Heller F, Boirivant M, Leon F, Yoshida M, Fichtner-Feigl S, Yang Z, Exley M, Kitani A, Blumberg RS, Mannon P, Strober W. Nonclassical CD1d-restricted NK T cells that produce IL-13 characterize an atypical Th2 response in ulcerative colitis. J Clin Invest. 2004 May;113(10):1490-7.

51. Arrieta MC, Bistritz L, Meddings JB. Alterations in intestinal permeability. Gut. 2006 Oct;55(10):1512-20

52. Feagan BG. Maintenance therapy for inflammatory bowel disease. Am J Gastroenterol. 2003 Dec;98(12 Suppl):S6-S17.

53. Sandborn WJ. Treatment of ulcerative colitis with oral mesalamine: advances in drug formulation, efficacy expectations and dose response, compliance, and chemoprevention. Rev Gastroenterol Disord. 2006 Spring;6(2):97-105.

54. Siegel CA, Sands BE. Review article: practical management of inflammatory bowel disease patients taking immunomodulators Aliment Pharmacol Ther. 2005 Jul 1;22(1):1-16.

55. Billioud V, Sandborn WJ, Peyrin-Biroulet L. Loss of response and need for adalimumab dose intensification in Crohn's disease: a systematic review. Am J Gastroenterol. 2011 Apr;106(4):674-84. Epub 2011 Mar 15.

56. Melgar S, Karlsson L, Rehnström E, Karlsson A, Utkovic H, Jansson L, Michaëlsson E. Validation of murine dextran sulfate sodium-induced colitis using four therapeutic agents for human inflammatory bowel disease. Int Immunopharmacol. 2008 Jun;8(6):836-44

57. Dawson DJ, Lobley RW, Burrows PC, Notman JA, Mahon M, Holmes R. Changes

in jejunal permeability and passive permeation of sugars in intestinal biopsies in coeliac disease and Crohn's disease. Clin Sci (Lond). 1988 Apr;74(4):427-31

58. Vilela EG, Torres HO, Ferrari ML, Lima AS, Cunha AS. Gut permeability to lactulose and mannitol differs in treated Crohn's disease and celiac disease patients and healthy subjects. Braz J Med Biol Res. 2008 Dec;41(12):1105-9
59. Madsen KL, Doyle JS, Jewell LD, Tavernini MM, Fedorak RN. Lactobacillus species prevents colitis in interleukin 10 gene-deficient mice. Gastroenterology. 1999 May;116(5):1107-14
60. Olson TS, Reuter BK, Scott KG, Morris MA, Wang XM, Hancock LN, Burcin TL, Cohn SM, Ernst PB, Cominelli F, Meddings JB, Ley K, Pizarro TT. The primary defect in experimental ileitis originates from a nonhematopoietic source. J Exp Med. 2006 Mar 20;203(3):541-52
61. Resta-Lenert S, Smitham J, Barrett KE. Epithelial dysfunction associated with the development of colitis in conventionally housed mdr1a-/- mice. Am J Physiol Gastrointest Liver Physiol. 2005 Jul;289(1):G153-62. Epub 2005 Mar 17.
62. Hollander D, Vadheim CM, Brettholz E, Petersen GM, Delahunty T, Rotter JI. Increased intestinal permeability in patients with Crohn's disease and their relatives. A possible etiologic factor. Ann Intern Med. 1986 Dec;105(6):883-5
63. Munkholm P, Langholz E, Hollander D, Thornberg K, Orholm M, Katz KD, Binder V. Intestinal permeability in patients with Crohn's disease and ulcerative colitis and their first degree relatives. Gut. 1994 Jan;35(1):68-72
64. Ikari A, Nagatani Y, Tsukimoto M, Harada H, Miwa M, Takagi K. Sodium-dependent glucose transporter reduces peroxynitrite and cell injury caused by cisplatin in renal tubular epithelial cells. Biochim Biophys Acta. 2005 Nov 30;1717(2):109-17.
65. Palazzo M, Gariboldi S, Zanobbio L, Selleri S, Dusio GF, Mauro V, Rossini A, Balsari A, Rumio C. Sodium-dependent glucose transporter-1 as a novel

immunological player in the intestinal mucosa.J Immunol. 2008 Sep 1;181(5):3126-36. Erratum in: J Immunol. 2008 Nov 15;181(10):7428.

66. Zanobbio L, Palazzo M, Gariboldi S, Dusio GF, Cardani D, Mauro V, Marcucci F, Balsari A, Rumio C. Intestinal glucose uptake protects liver from lipopolysaccharide and D-galactosamine, acetaminophen, and alpha-amanitin in mice.Am J Pathol. 2009 Sep;175(3):1066-76.
67. Wright EM, Loo DD, Hirayama BA. Biology of human sodium glucose transporters. Physiol Rev. 2011 Apr;91(2):733-94.
68. Sala-Rabanal M, Hirayama BA, Loo DD, Chaptal V, Abramson J, Wright EM. Bridging the gap between structure and kinetics of human SGLT1. Am J Physiol Cell Physiol. 2012 May 1;302(9):C1293-305.
69. Raja MM, Kinne RK. Interaction of C-terminal loop 13 of sodium-glucose cotransporter SGLT1 with lipid bilayers. Biochemistry. 2005 Jun 28;44(25):9123-9.
70. Tyagi NK, Puntheeranurak T, Raja M, Kumar A, Wimmer B, Neundlinger I, Gruber H, Hinterdorfer P, Kinne RK. A biophysical glance at the outer surface of the membrane transporter SGLT1. Biochim Biophys Acta. 2011 Jan;1808(1):1-18.
71. La Ferla B, Spinosa V, D'Orazio G, Palazzo M, Balsari A, Foppoli AA, Rumio C, Nicotra F. Dansyl C-glucoside as a novel agent against endotoxic shock. ChemMedChem. 2010 Oct 4;5(10):1677-80.
72. Gorboulev V, Schürmann A, Vallon V, Kipp H, Jaschke A, Klessen D, Friedrich A, Scherneck S, Rieg T, Cunard R, Veyhl-Wichmann M, Srinivasan A, Balen D, Breljak D, Rexhepaj R, Parker HE, Gribble FM, Reimann F, Lang F, Wiese S, Sabolic I, Sendtner M, Koepsell H. Na(+)-D-glucose cotransporter SGLT1 is pivotal for intestinal glucose absorption and glucose-dependent incretin secretion. *Diabetes* 2012;61(1):187-96.

73. Lin R, Murtazina R, Cha B, Chakraborty M, Sarker R, Chen TE, Lin Z, Hogema BM, de Jonge HR, Seidler U, Turner JR, Li X, Kovbasnjuk O, Donowitz M. D-glucose acts via sodium/glucose cotransporter 1 to increase NHE3 in mouse jejunal brush border by a Na+/H+ exchange regulatory factor 2-dependent process. *Gastroenterology* 2011;140(2):560-71.
74. Shenolikar S, Weinman EJ. NHERF: targeting and trafficking membrane proteins. *Am J Physiol Renal Physiol* 2001;280(3):F389-95.
75. Fouassier L, Duan CY, Feranchak AP, Yun CH, Sutherland E, Simon F, Fitz JG, Doctor RB. Ezrin-radixin-moesin-binding phosphoprotein is expressed at the apical membrane of rat liver epithelia. *Hepatology* 2001;33(1):166-76.
76. Hu Z, Wang Y, Graham WV, Su L, Musch MW, Turner JR. MAPKAPK-2 is a critical signaling intermediate in NHE3 activation following Na+-glucose cotransport. *J Biol Chem* 2006;281(34):24247-53.
77. Wu KL, Khan S, Lakhe-Reddy S, Jarad G, Mukherjee A, Obejero-Paz CA, Konieczkowski M, Sedor JR, Schelling JR. The NHE1 Na+/H+ exchanger recruits ezrin/radixin/moesin proteins to regulate Akt-dependent cell survival. *J Biol Chem* 2004;279(25):26280-6.
78. Keefe DM, Brealey J, Goland GJ, Cummins AG. Chemotherapy for cancer causes apoptosis that precedes hypoplasia in crypts of the small intestine in humans. *Gut* 2000;47(5):632-7.
79. Gibson RJ, Keefe DM. Cancer chemotherapy-induced diarrhoea and constipation: mechanisms of damage and prevention strategies. *Support Care Cancer* 2006;14(9):890–900
80. Sonis ST. Mucositis as a biological process: a new hypothesis for the development of chemotherapy-induced stomato- toxicity. Oral Oncol 1998;34(1):39–43) ,

81. Gibson RJ, Keefe DM, Lalla RV, Bateman E, Blijlevens N, Fijlstra M, King EE, Stringer AM, van der Velden WJ, Yazbeck R, Elad S, Bowen JM; For The Mucositis Study Group of the Multinational Association of Supportive Care in Cancer/International Society of Oral Oncology (MASCC/ISOO). Systematic review of agents for the management of gastrointestinal mucositis in cancer patients. *Support Care Cancer* 2012 Nov 10.
82. Zhao H, Zhang H, Wu H, Li H, Liu L, Guo J, Li C, Shih DQ, Zhang X. Protective role of 1,25(OH)2 vitamin D3 in the mucosal injury and epithelial barrier disruption in DSS-induced acute colitis in mice. BMC Gastroenterol. 2012 May 30;12:57.
83. Feighery LM, Smith P, O'Mahony L, Fallon PG, Brayden DJ. Effects of Lactobacillus salivarius 433118 on intestinal inflammation, immunity status and in vitro colon function in two mouse models of inflammatory bowel disease. Dig Dis Sci. 2008 Sep;53(9):2495-506. Epub 2007 Dec 20.
84. Rose WA 2nd, Sakamoto K, Leifer CA. Multifunctional role of dextran sulfate sodium for in vivo modeling of intestinal diseases. BMC Immunol. 2012 Aug 1;13:41. doi: 10.1186/1471-2172-13-41.